



HAL
open science

Global regulation via modulation of ribosome pausing by EttA

Fares Ousalem, Saravuth Ngo, Thomas Oiffer, Amin Omairi-Nasser, Marion Hamon, Laura Monlezun, Gregory Boel

► **To cite this version:**

Fares Ousalem, Saravuth Ngo, Thomas Oiffer, Amin Omairi-Nasser, Marion Hamon, et al.. Global regulation via modulation of ribosome pausing by EttA. 2023. hal-04249747

HAL Id: hal-04249747

<https://hal.science/hal-04249747v1>

Preprint submitted on 19 Oct 2023

HAL is a multi-disciplinary open access archive for the deposit and dissemination of scientific research documents, whether they are published or not. The documents may come from teaching and research institutions in France or abroad, or from public or private research centers.

L'archive ouverte pluridisciplinaire **HAL**, est destinée au dépôt et à la diffusion de documents scientifiques de niveau recherche, publiés ou non, émanant des établissements d'enseignement et de recherche français ou étrangers, des laboratoires publics ou privés.

Global regulation via modulation of ribosome pausing by EttA

**Farès Ousalem^{1§}, Saravuth Ngo¹, Thomas Oïffer¹, Amin Omairi Nasser¹,
Marion Hamon², Laura Monlezun¹, Grégory Boël^{1,*}**

¹Expression Génétique Microbienne, CNRS, Université Paris Cité, Institut de Biologie Physico-Chimique, Paris, France. ²Centre National de la Recherche Scientifique (CNRS), Institut de Biologie Physico-Chimique, Plateforme de Protéomique, FR550, F-75005 Paris, France.

* To whom correspondence may be addressed:

Grégory Boël, Institut de Biologie Physico-Chimique, 13 rue Pierre et Marie Curie, 75005 Paris, France, Tel: +33-1-58415121; e-mail: boel@ibpc.fr

Keywords: Protein synthesis, Acidic residues translation stalling, ABC-F protein family, TCA cycle, glyoxylate shunt.

§ Current address: Biomarqueurs et nouvelles cibles thérapeutiques en oncologie, INSERM U981, Université Paris Saclay, Institut de Cancérologie Gustave Roussy, 11 rue Edouard Vaillant, 94805 Villejuif Cedex, France

Abstract

Having multiple rounds of translation of the same mRNA is a key feature of the Central Dogma that creates substantial dynamic complexities along with opportunities for regulation related to ribosome pausing and stalling at specific sequences¹⁻⁵. The molecular mechanisms controlling these critical processes and the principles guiding their evolution remain among the least understood facets of cellular physiology. We herein use a combination of genetic, genomic, physiological, and biochemical methods to show that regulation of ribosome pausing at specific amino acid sequences can produce ~2-fold changes in protein expression levels that have a strong influence on cell growth and therefore evolutionary fitness. We demonstrate, both *in vivo* and *in vitro*, that the ABCF protein EttA^{6,7} directly controls the translation of mRNAs coding for a subset of enzymes in the tricarboxylic acid (TCA) cycle and its glyoxylate shunt, which dramatically modulates growth in some chemical environments. It also modulates expression of specific proteins involved in metabolically related physiological and stress-response pathways. These regulatory activities are mediated by EttA rescuing ribosomes paused at specific patterns of negatively charged residues within the first 30 amino acids of nascent proteins. The previously established dependency of EttA's activity on ADP:ATP ratio^{6,7} can modulate these effects based on cellular energy status. We thus establish a new global regulatory paradigm based on sequence-specific modulation of translational pausing.

Main

The ATP binding protein F (ABC-F) family, belonging to the ABC superfamily⁸, constitutes a group of proteins where all the members studied to date are involved in ribosome-related functions^{6,7,9-12,9-21}. They are widespread in bacteria and eukaryotes and in general, paralogues are present in the same organism, such as *E. coli* which has four ABC-F proteins: EttA, Uup, YheS and YbiT^{6,13,21-23}.

ABC-F proteins are composed of two ABC domains in tandem connected together by a linker region that contains the P-site tRNA Interaction Motif (PtIM)^{6,14,21,23,24}, a signature motif of the family defined by the Pfam database²⁵ as ABC_tran_Xtn (PF12848). Each ABC-domain carries consensus Walker A and B motifs and in the presence of ATP the two domains come together, binding two ATP molecules to shape an ATP-bound closed conformation^{21,23,26}. In this conformation, ABC-F proteins bind to the E site of the 70S ribosome^{6,7,10,16,17,19,20} and require the hydrolysis of the ATP molecules to dissociate from the ribosome⁶. Consequently, an ATPase-deficient mutant, in which the two catalytic glutamates of each Walker B motif of the ABC domain are replaced by glutamines (EQ₂ mutant)²⁶, forms a stable complex with the ribosome^{6,7,10,13,19,20}. This stabilization leads to an inhibition of protein synthesis and an arrest of bacterial growth^{6,13,22}. To date, twelve cryo electron microscopy structures of ABC-F proteins in complex with the 70S ribosome are known. These structures reveal an overall geometry with similar contacts between the protein and the ribosome, but the corresponding regions of each ABC-F that contact the ribosome differ in sequences^{7,10,12,16,19,20,23,27}. The PtIM extension points towards the peptidyl transfer center (PTC) of the ribosome, but shows considerable variation in length^{10,16,17,19-21,28}. With the EF-P/eIF-5A protein that has been identified to rescue ribosomes stalled due to the synthesis of polyproline-containing proteins²⁹⁻³¹ the ABC-F are the only factors that bond to the ribosomal E site.

Some ABC-F have a clear physiological function such as the antibiotic resistance ABC-F (ARE ABC-F) factors^{9,10,12,14-20,32,33} which provide resistance toward antibiotics that target the PTC

and the nascent peptide exit tunnel (NPET) of the ribosome^{9,10,12,16,17,19,20}. However, for most of the family, their physiological function remains unclear. In eukaryotes, ABC-F proteins are associated with pleiotropic effects. In Yeast the N-terminal domain of GCN20 is involved in the regulation of translation upon amino-acid starvation^{34,35}. The second yeast ABC-F, ARB1, is an essential gene important for ribosome biogenesis³⁶ and the corresponding protein has been identified in the cryo-EM structure of the 60S ribosomal quality control complex in a pre-peptidyl-tRNA cleavage state²⁸. The human ABC50 (ABC-F1) protein influences translation initiation *in vitro* at an internal ribosome entry site of mRNA³⁷ and also functions as an E2 Ubiquitin-conjugating enzyme in the regulation of the inflammatory response in macrophages³⁸. The three human ABC-F paralogues have been detected in processes involved in immune responses³⁹⁻⁴⁴ and cancer developments and treatments^{42,45-52}, but their mechanism of action is unknown. In prokaryotes, all the structurally studied ABC-F can adjust the conformation of the PTC and/or the positioning of the P-site tRNA^{13,23} (and some affect bacterial fitness²²). Based on biochemical and structural studies of the EttA protein, we previously proposed a model in which EttA regulates the first step of translation depending on the ADP:ATP ratio in the reaction^{6,7} and showed that loss of EttA resulted in reduced competitive fitness in stationary phase⁶. However, important questions remained: what is the physiological role of EttA in *E. coli* and does its action impact translation of all mRNA?

In this study we have used an unbiased approach to determine the impact of the *ettA* deletion ($\Delta ettA$) on the physiology of *E. coli*. The gene deletion creates a hypersensitivity to salt when the bacteria are grown on carbon sources metabolized by the TCA cycle. This phenotype is due to the reduced translation of several genes of the TCA cycle and of genes involved in stress responses. For eight of them, we show that the reduced synthesis occurs during translation of their mRNAs when the newly polymerized protein contains acidic-amino acids within the first 30 amino acids i.e. before the elongating peptide reaches the end of the ribosomal NPET. We demonstrate that changes in the expression of *aceB* and *aceA* can explain most of the phenotypes we observed.

In addition, we show that over-expression of *mgtA* gene (encoding a Mg²⁺ transporter) in the Δ *ettA* strain is due to the action of EttA on the Intrinsic Ribosome Destabilization (IRD) effect of the leader peptide MgtL which regulates *mgtA* expression³.

Loss of ettA impairs bacterial metabolic adaptation and alters protein expression patterns. Our investigation of the physiological function of EttA started with the previously reported phenotype of competitive fitness defect of the *ettA* deleted strain (Δ *ettA*) during extended stationary phase in LB⁶. In our replication of the experiment we discerned the phenotype's dependency on the source of the LB medium used (**Extended Data Fig. 1a**). Subsequently, we have now developed a MOPS-Tricine buffered minimal medium where the phenotype is enhanced, first by reducing the amount of inorganic phosphate, then by using amino acids (aa) as carbon source (MMAA medium) and finally by adding NaCl (0.4 M) to the medium (MMAA-NaCl). In this last condition, there was a rapid loss in competitive fitness of the Δ *ettA* strain compared to the previous condition (1 day vs 3 days) (**Extended Data Fig. 1a**). In this work we have systematically compared three strains MG1655 WT, Δ *ettA* and the Δ *ettA* complemented with an exogenous chromosomal copy of *ettA* (*C_{ettA}*). In the MMAA medium, all 3 strains doubled every 3 h, whereas in the MMAA-NaCl medium the doubling time of the WT and the complemented strains increased to 8 h (**Fig. 1a**) while that of the Δ *ettA* strain was more than 9 h and exhibited a much longer lag time (5 h) compared to the two other strains (**Fig. 1a**). Strains deleted for the other *E. coli* ABC-F genes, grew like the WT, showing that this phenotype is specific to *ettA* (**Extended Data Fig. 1b**). Noticeably, addition of NaCl induced EttA expression as shown using a translational *yfp* (Yellow Fluorescent Protein) reporter fused to *ettA* gene (**Fig. 1b and Extended Data Fig. 1c**).

Proteomic studies were performed on the supernatant (S₁₅) or pellet (P₁₅₀) fractions from protein extracts from cultures grown in MMAA-NaCl medium, which identified several differences in protein expression in the Δ *ettA* strain compared to the WT or the *C_{ettA}* strains (**Extended Data Fig. 1d, e**). Coupled with transcriptomic studies on the same cell extracts and

focusing on proteins under-expressed in the $\Delta ettA$ strain, we identified different scenarios: For *aceB*, *aceA* and *fumC* genes the corresponding mRNA was expressed at the same level as the WT suggesting a posttranscriptional regulation (**Extended Data Fig. 1f**). For *rraB*, *yjbJ*, *elaB*, and *hchA* genes, mRNA levels and protein decreased, we hypothesized that the mRNA decay was related to translation because there is an intrinsically close relation between the translation of an mRNA and its stability⁵³⁻⁵⁶. For other genes, a dominant positive effect on the transcription was observed as, for example, *mgtA*, for which the mechanism of regulation by EttA will be described below. A down-regulation can also be seen for most of the flagella regulon genes, in the $\Delta ettA$ strain, suggesting a defect in motility in this strain that was validated by motility assays (**Extended Data Fig. 1g, h**).

We confirmed the decrease in expression in the $\Delta ettA$ strain for five genes (*aceB/A*, *fumC*, *yjbJ* and *hchA*) using a *yfp* reporter where the *yfp* gene, without its initiation codon, was inserted just before the stop codon of the tested genes. The fluorescence level was lower for each construct in the $\Delta ettA$ strain (**Fig. 1c and Extended Data Fig. 2a**) as well as the protein level quantified by western blot (**Extended Data Fig. 2b**). For *aceB/A* and *fumC* there was no change in their transcription level as determined by northern blot, but for *yjbJ* and *hchA* transcript levels decreased in the $\Delta ettA$ strain. Other related genes of the metabolic pathway were tested, but they either did not show any change between the strains (*maeB*, *fumB*, *frdB*) or the fluorescence levels were too low to be quantified (*frdA/C/D*, *glcB* and *elaB*) (**Extended Data Fig. 2a**).

Since the phenotype of the $\Delta ettA$ strain arises when aa, which are primarily metabolized by the TCA cycle⁵⁷, are used as carbon source, we tested media with single TCA intermediates as carbon sources. This screen (**Fig. 1c and Extended Data Fig. 1i**) showed that the growth inhibition by salt in the $\Delta ettA$ strain occurs specifically when malate, fumarate and succinate were used. To our surprise, growth on glyoxylate produced a reversed phenotype where $\Delta ettA$ grew faster than the other strains.

EttA alleviates ribosome pausing on acidic residues. In a second approach to disengage the five validated *yfp*-reporter fusions from their genomic transcriptional environment, we inserted their sequences from the 5' untranslated region (UTR) of target genes to the *yfp* stop codon in a low copy plasmid (pMMB) under control of an IPTG inducible promoter. The constructs for *aceB*, *fumC*, *hchA* and *yjbJ*, which showed lower expression in the $\Delta ettA$ strain from their own promoter, also showed lower expression after IPTG induction of the pMMB plasmid in the $\Delta ettA$ compared to the WT or the C_{ettA} strains, but constructions harboring only the 5'UTR up to the initiation codon of *aceB* or *yjbJ* were expressed independently of EttA (**Extended Data Fig. 3a, b**) showing that the translated sequence is necessary for regulation by EttA.

Next, we made truncations within the target genes in order to determine the minimal sequence that is required for the EttA-dependent expression change (**Fig. 2a and Extended Data Fig. 3a, b**). Constructs with the first 10 or 60 residues of AceB were still subjected to EttA regulation, whereas the construct with only the first eight residues had lost it. The residues absent in this construct, Asp9 and Glu10, are both acidic residues and their replacement by the neutral residues Asn and Gln respectively, also abolished the differential expression in the $\Delta ettA$ strain. The replacement of one acidic residue reduced the EttA-dependent effect, but two, completely abolished it (**Fig. 2a and Extended Data Fig. 3a, b**). For AceB, the replacement of the three threonines, that precede the acidic residues, by alanine did not affect the regulation. The gene *aceA* is in an operon after the gene *aceB* and the regulation by EttA was observed only when *aceA:yfp* was expressed as part of the *aceBA* operon, implying a co-translation of the two genes (**Fig. 2a and Extended Data Fig. 3a, b**), the translation of *aceA* being dependent of the rate of translation of *aceB*.

For *fumC*, *yjbJ* and *hchA* genes, the EttA driven regulation was also maintained in constructs that contain at least the first 5-20 N-terminal residues of the encoded protein sequences (FumC: 10 aa, YjbJ: 5 aa and HchA: 20 aa). For these three genes, replacement of two acidic residues (Asp4 Glu5 for YjbJ, Glu7 Asp9 for FumC and Glu15 Asp16 for HchA) by neutral

residues (Asn for Asp and Gln for Glu) abolished the regulation by EttA (**Fig. 2a and Extended Data Fig. 3a and b**). Overall, these results strongly suggest that EttA can facilitate the translation of mRNA encoding acidic residue repeats at the beginning of their sequence.

In light of these findings, we revisited a subset of our early proteomic targets some of which we had not previously examined or could not detect the expression with our YFP fusion reporters (**Extended Data Fig. 2a**). We noticed that FrdD, ElaB and RraB contain two or three acidic residues early in their sequences (Asp10 Glu11 for FrdD, Asp11 Asp12 Asp13 for ElaB and Glu8 Glu9 for RraB). We applied the same plasmid-based expression approach to those targets and showed that YFP reporters containing the early part of the target's sequences (FrdD 14 aa, ElaB 15 aa and RraB 10 aa) exhibited a dependency on EttA for their expression. Moreover, the replacement of the acidic residues by neutral ones eliminated the EttA dependency (**Fig. 2a and Extended Data Fig. 3a, b**).

In order to demonstrate the translational regulation driven by EttA, we performed *in vitro* translation assays (IVTAs) with mRNA corresponding to the shortest YFP constructs that showed the EttA-dependent differential expression (*aceB*_{1-10aa}, *yjbJ*_{1-5aa} and *rraB*_{1-10aa}) and with their corresponding mutants that alleviated it (*aceB*-NQ_{1-10aa}, *yjbJ*-NQ_{1-5aa} and *rraB*-QQ_{1-10aa}). For all the genes, IVTA expression on the WT RNA sequence was increased when some purified partially monomeric His₆-EttA protein (**Extended Data Fig. 4a**) was added, whereas there was no effect of His₆-EttA on mRNAs where the acidic amino acids had been replaced by neutral residues (**Fig. 2b and Extended Data Fig. 4b**).

To investigate if the acidic residues produce a stalling of the ribosome during translation of the mRNA, we performed some toeprinting assays. Initially we used retapamulin and thiostrepton, two antibiotics which stall ribosomes at start codons, to confirm the translational start site (**Fig. 2c**). The toeprint of the *aceB*_{1-10aa} and the *aceB*-NQ_{1-10aa} constructs were similar in the absence of EttA. The addition of EttA had no effect, but EttA-EQ₂ produced two stalling events. One at the initiation site on both WT and mutant constructs, consistent with previous results

demonstrating that EttA-EQ₂ binds to ribosomes with a free E site, *i.e.* primarily initiating ribosomes^{6,7,19,20}. The second stalling event, only present in the *aceB*_{1-10aa} construct, was identified 24 nt after the initiation toeprinting, which corresponds to the Asp9 codon in the ribosomal P-site. In contrast, *yjbJ* toeprinting (**Fig. 2d**) showed a specific stalling on WT *yjbJ*_{1-5aa} in addition to the toeprint band of the initiation complex (determined here by toeprinting the in presence of EttA-EQ₂ which induced stalling at initiation). This second toeprint signal was not observed when WT EttA was added-but was still faintly detected with EttA-EQ₂. This toeprint signal is located 7 nt from the initiation toeprinting, which makes it unclear if the stalling occurred with Lys3 or Asp4 in the P site of the ribosome. We tested if Lys3 had an effect on the regulation by EttA by replacing it by an Ala in our *yjbJ*_{1-5aa}:*yfp* reporter (**Fig. 2a and Extended Data Fig. 3a**). The related construct showed the same decrease in expression in the absence of EttA as the WT construct *in vivo*, demonstrating that Lys3 has no impact on the EttA-dependent regulation.

Altogether these results argue that polymerization of acidic residues triggers ribosome pausing, manifesting in two potential outcomes. Firstly, in the case of *aceB*, the absence of a toeprint signal in the absence of EttA, juxtaposed with its presence in the presence of His₆-EttA-EQ₂, strongly suggests ribosome dissociation that can be stabilized by EttA-EQ₂. Secondly, for *yjbJ*, a distinct ribosome stalling event is observed, characterized by the detectable toeprinting signal. Notably, EttA is consistently demonstrated as an effective modulator, successfully mitigating ribosomal pausing and thereby augmenting protein expression in all instances. These observations are in agreement with recent reports showing that repeated acidic residues can lead to intrinsic ribosome destabilization^{2,3}.

Regulation of AceA and AceB expression by EttA explains most observed phenotypes.

Three of the proteins for which the synthesis is directly regulated by EttA: AceB (malate synthase), FumC (fumarase C) and FrdD (fumarate reductase subunit D), are enzymes of TCA and glyoxylate shunt pathways. More specifically, they catalyze reactions that use the substrates for which we

identified a growth phenotype for the $\Delta ettA$ strain (**Fig. 1c**). A fourth enzyme, AceA (isocitrate lyase) is indirectly regulated by EttA through the regulation of *aceB*, the upstream gene of the operon (**Fig. 2a**). AceA catalyzes the conversion of isocitrate into succinate and glyoxylate while AceB catalyzes the conversion of glyoxylate and acetyl-CoA into malate and CoA. Together they form the glyoxylate shunt, a metabolic pathway found in some bacteria and plants that bypass the carbon dioxide-producing steps of the TCA cycle (**Fig. 1c**).

However in *E. coli* the major route to metabolize glyoxylate, is not by converting it to malate by AceB, but by using glyoxylate carboligase⁵⁸⁻⁶¹ (Gcl) to condense two glyoxylates into tartronate semialdehyde, which is incorporated into the glycolysis pathway by its conversion to glycerate and then to 2-phosphoglycerate^{62,63} (**Fig. 3a**). Accordingly, a deletion of the *gcl* gene is expected to have a drastic effect on *E. coli* growth on glyoxylate and indeed abolished the growth of the three strains on MM with this carbon source (**Fig. 3a and Extended Data Fig. 5a**). We hypothesized that the repression of AceB expression (35% less in $\Delta ettA$ strain) would promote the metabolic flux toward the *gcl* pathway, thus increasing the growth of the $\Delta ettA$ strain on glyoxylate (**Fig. 3b**). If so, deletion of *aceB* should increase growth on glyoxylate for all the strains and over-expression should produce the reverse effect. This prediction was confirmed experimentally, where the deletion of *aceB* increased the growth and all the strains grew at the same rate (**Fig. 3a and Extended Data Fig. 5a**). Over-expression of *aceB* reduced the growth rate for all the strains, but the $\Delta ettA$ strain retained a small advantage of growth. Over-expression of the AceB-NQ variant, for which EttA had no effect on its expression (**Fig. 2a**), also reduced the growth rate of all the strains, but equally in all three strains (**Fig. 3a and Extended Data Fig. 5a**), as expected if the phenotype was due to the regulation of AceB by EttA. The deletion of the second malate synthase gene (*glcB*), which is expressed at low level in our experimental conditions (**Extended Data Fig. 2a**), also improved growth of all the strains on glyoxylate, but the $\Delta ettA$ strain maintained a small advantage (**Fig. 3a and Extended Data Fig. 5a**).

To understand the metabolic problem caused by the loss of EttA we tested growth of the

strains deleted for genes encoding TCA enzymes in MMAA NaCl. First, deletion of *aceA* had no effect on growth in MMAA medium, but addition of NaCl at 0.4 M prevented the growth of the three strains, suggesting that *aceA* is essential for salt stress in this condition (**Fig. 3a and Extended Data Fig. 5b, c**). The glyoxylate shunt has been previously identified for its importance in tolerance to desiccation⁶⁴ and, in plants, to salt⁶⁵. Overall, the results suggest that during salt stress, the Δ *ettA* strain uses less the glyoxylate shunt pathway and therefore probably funnels more metabolic flux through the TCA cycle (**Fig. 3c**). Accordingly, a deletion of the *icd* gene (isocitrate dehydrogenase), which prevents the metabolic flux through the carbon dioxide-producing steps of the TCA cycle, increased the salt sensibility of the Δ *ettA* strain as did the deletion of *fumC* and *frdD* (**Fig. 3a and Extended Data Fig. 5b**). Deletion of *aceB* did not affect the growth phenotype, while overexpression of *aceA* reduced the phenotype (**Fig. 3 and Extended Data Fig. 5b**). This supports the idea that the Δ *ettA* strain defect is partly due to the lower expression of *aceA*. Finally, deletion of *gcl* severely inhibited the growth of the WT and *C_{ettA}* strains in presence of NaCl, suggesting that they use the conversion of glyoxylate to tartronate semialdehyde in the high salt condition more than the Δ *ettA* strain in the high salt condition (without salt, the deletion had no effect on the growth) (**Fig. 3a and Extended Data Fig. 5b**). This observation is also in agreement with the Δ *ettA* strain using principally the TCA cycle and the WT using more the glyoxylate to tartronate semialdehyde pathway. This could be beneficial under salt stress because it could reduce respiration by funneling the metabolic flux towards mixed acid fermentation and/or by increasing synthesis of osmoprotectants by the gluconeogenesis pathway (**Fig. 3c**).

Change of *mgtA* expression is due to the action of *EttA* on the translation of the leader peptide *MgtL*. The proteomic study on the P₁₅₀ protein extracts, which included membrane proteins, showed a 3-fold increase in the Δ *ettA* strain of the protein MgtA, an ATP-dependent Mg²⁺ importer⁶⁶. The expression of the gene *mgtA* is under the regulation of the leader peptide MgtL^{3,67,68}. During cellular growth in conditions where Mg²⁺ is not limited, translation of *mgtL* by

the ribosome maintains a Rho-dependent terminator (RDT)^{3,67,68} accessible to terminate the transcription of the mRNA and therefore prevents the transcription of *mgtA* (**Fig. 4a**). When Mg²⁺ becomes limiting, the low intracellular concentration favors ribosome dissociation during the translation of *mgtL*. This ribosomal drop-off occurs during the translation of the destabilizing motif EPDP and leads to a conformational change of the mRNA that prevents accessibility to the RDT and transcription termination³, therefore *mgtA* is transcribed (**Fig. 4a**). To test if EttA could modulate the translation of *mgtL* and consequently the transcription of *mgtA*, we constructed two reporters using the same plasmid, one with the sequence of *mgtL* (from the 5'UTR to the codon before the stop codon) fused to the *yfp* and the other one from the same 5'UTR extended to the 5th codon of *mgtA* fused to the *yfp* (**Fig. 4b and Extended Data Fig. 6a**). When strains were grown in the MMAA medium with 2 mM or 0.05 mM of Mg²⁺, the fluorescence signal was lower in the Δ *ettA* strain for the *mgtL* fusion and higher for the *mgtA*_{1-5aa} fusion, in accordance with an action of EttA on the leader peptide MgtL. Also, we showed by northern blot that *mgtA*_{1-5aa} transcript increased in the Δ *ettA* strain (**Extended Data Fig. 6c**), consistent with the previously reported transcription termination regulation driven by *mgtL* translation^{3,68}. Replacing Glu2 and Asp4 of MgtL with Gln and Asn, respectively, resulted in an increased expression of MgtL fusion in the Δ *ettA* strain, while MgtA fusion showed no detectable expression, as expected (**Fig. 4b and Extended Data Fig. 6a, b**).

We used IVTA to determine if EttA directly regulated *mgtL* expression (**Fig. 4c and Extended Data Fig. 6d**) and confirmed that *mgtL* expression was increased in the presence of EttA, but not for the *mgtL* variant where the acidic residues were replaced. Toeprinting performed on the same constructs showed a toeprint signal, corresponding to a ribosome stalled with Pro3 in the ribosomal P-site in the presence of His₆-EttA, which is even more pronounced in the presence of His₆-EttA-EQ₂. This toeprint signal occurred only for the WT *mgtL* construct (**Fig. 4d**). These observations suggest that EttA can stabilize the ribosome to prevent the drop-off and therefore repress *mgtA* transcription.

The acidic residues need to be within the 30 first aa of the sequence for protein synthesis to be EttA-dependent. We have identified eight proteins for which the synthesis is dependent on EttA and for all of them acidic residues are necessary for this effect. Therefore, we aimed to design a consensus motif containing the acidic residues and few neighboring ones. The consensus, derived from the 8 sequences sequence NKDEPD, which is not present in the *E. coli* proteome, was inserted after the initiating methionine of the YFP sequence on two different constructs: one with the 5'UTR of *aceB* and the other one with the 5'UTR of *yjbJ*. Both constructs showed a strong EttA dependency on expression (**Fig. 5a and Extended Data Fig. 7a, b**), confirming that we can design an artificial sequence that needs EttA for optimal expression. By reproducing the effect *in vitro* in an IVTA using the 5'UTR *aceB* construct, we confirmed that this occurred by direct interaction of EttA on the translating ribosome (**Fig. 5b and Extended Data Fig. 7c**). We tested a construct that expressed the same aa sequence but used different synonymous codons (syn-codons). This construct had a drop in the overall expression level, but the EttA dependency on expression was maintained, therefore the EttA regulatory effect is dependent on the aa, but not on the codons used (**Fig. 5a and Extended Data Fig. 7a, b**).

To determine if the position of this sequence had an importance for the EttA-dependent expression, we tested several constructs where this sequence was moved by increments of 10 aa away from the initiating methionine. We used the sequence of AceB-NQ, whose expression is no longer EttA-dependent, to test the 10 aa increments. Displaced by 10 aa, the consensus sequence still produced a strong induction by EttA. When displaced by 20 aa, there was only a small induction by EttA while at 30 and 40 aa there was no effect of EttA (**Fig. 5a and Extended Data Fig. 7a, b**). This experiment demonstrated that the acidic residues need to be within the first 30 aa of a protein sequence to make its expression EttA-dependent.

Since we found that two acid residues in the beginning of the sequence can make protein synthesis dependent on EttA, we wondered if it could be detected genome-wide in our proteomic

studies. We searched for the presence of a motif where two acidic residues are adjacent or separated by one aa in the first 50 aa of *E. coli* proteome (Motif: $-/X_{0,1}/-$). Then we grouped them according to the position of the acidic residues within segments of 10 aa and compared the ratio of expression of the WT versus the $\Delta ettA$ or C_{ettA} strains (**Fig. 5c and Extended Data Fig. 7d**). This analysis revealed that the presence of the motif within the first 20 aa correlated with a statistically significant decrease of expression only in the $\Delta ettA$ strain and with a stronger effect when it is located within the first 10 aa.

The analysis of the proteomic data also revealed that certain proteins containing double acidic residues early in their sequences remain unaffected by *ettA* deletion. Furthermore, the YFP sequence begins with "MVSKGEE," and its expression remains unaffected by EttA (**Extended Data Fig. 7e, f**). We attempted to render YFP expression dependent on EttA by introducing sequential mutations in the acidic residues and their surroundings (**Extended Data Fig. 7e, f**). Neither the EE nor DE motif alone led to EttA dependency. Even though the ED motif showed a statistically significant change, it was only around 7%, which is less than changes observed with EttA's physiological targets. In fact, at a minimum, a DPEE motif was necessary. The presence of a Pro suggests that a structural constraint on the positioning of the nascent peptide is crucial for this phenomenon to occur.

DISCUSSION

We have demonstrated that EttA enhances translation of specific mRNA (*aceB*, *rraB*, *yjbJ*, *fumC*, *frdD*, *hchA*, *elaB* and *mgtL*). This specificity is due to the destabilizing effect of early acidic residues during the synthesis of these proteins that is rescued by EttA. We propose a model (**Fig. 5d**) where EttA first binds to a ribosome paused at the acidic-residues repeat, most likely before the peptide bond formation of the second acidic residue occurs (**Fig. 2c, d and Fig. 4d**). From here it can prevent ribosome possible drop-off as illustrated by *aceB*, and *mgtL* (**Fig. 2c, Fig. 4d**) where the toeprinting didn't detect stalling in the absence of His₆-EttA, but did detect stalling with His₆-

EttA-EQ₂, suggesting that the non-hydrolytic EttA mutant can prevent the drop-off but cannot restore the elongation. For MgtL, ribosomal drop-off during elongation of acidic-residues has been previously reported³. In the case of *yjbJ* the stalling does not seem to lead to ribosomal drop-off since a clear stalling signal is seen on the toeprinting experiments in the absence of EttA (**Fig. 2d**). In the final step, EttA allows the elongation to restart.

This model resonates with the function of the translation factor EF-P⁶⁹, which enhances translation of polyproline-containing proteins^{29,30}. Polyproline-containing nascent chains adopt a conformation that is incompatible with the structure of the NPET of the ribosome, which therefore induces a tension on the peptidyl-tRNA⁷⁰ that prevents the formation of the peptide bond with the Pro-tRNA in the A site. EF-P binding to the stalled ribosome forces the polyproline-containing nascent chain to adopt a correct conformation. Although the structures of EF-P and EttA are not at all similar (**Extended Data Fig. 8a**), comparison of their complexes with the 70S ribosome^{23,70} aligned on domain V of 23S rRNA, reveals that the extension of EF-P that points toward the PTC and which contains the essential β -lysyl-lysine residue, aligns closely with the PtIM of EttA (**Fig. 5e and Extended Data Fig. 8b**). Thus, there are structural and functional similarities between EF-P and EttA in the part of the proteins that interacts with the acceptor stem of the P-site tRNA. Moreover, structures of EttA-EQ₂ in complex with initiating or elongating ribosomes²³ show the geometry of the P-site tRNA to be catalytically favorable for peptide bond formation, as observed for the structures of EF-P ribosomal complexes⁷⁰.

The translational stalling induced by polyproline is not systematic and it depends on both the position within the sequence⁷¹ and the sequence context upstream of the stall site⁷². A similar situation is observed for the acidic residues-induced stalling that are rescued by EttA. Although we have demonstrated that several proteins containing acidic residue repeats within the 30 first aa are dependent on EttA (**Fig. 2, Fig. 4b and Fig. 5a**), we have identified other proteins with this feature for which the expression is EttA-independent (**Fig. 5c**). Therefore, the mere presence of di-acidic residues is not sufficient to destabilize translating ribosome rendering the translation

EttA-dependent. Most likely, as in the case of polyproline, the conformation of the nascent peptide in NPET of the ribosome is important and the presence of a proline upstream of the acidic residues in four of our eight targets corroborates this hypothesis. Nevertheless, some fundamental differences exist between EF-P and EttA and the type of stalling rescued. The stalling induced by polyproline can occur after the nascent peptide has filled the entirety of the ribosomal NPET^{29,30,71,72}, whereas here in the case of acidic residues it is restricted to a partially filled NPET. For the rescue mechanism, EF-P operates by a simple binding to the stalled complex and induces fitting rescue⁷⁰. EttA on the other hand uses, after binding, its ATPase activity to possibly dynamically reshape the positioning of the nascent peptide in the NPET/PTC²³. Another difference is the positioning of the L1 stack. While EF-P can maintain it in an “in” conformation⁷⁰ (toward the E site), EttA exclusively places it in an “out” (away from the E site) conformation^{7,23}.

Our results echo the work of the Taguchi lab, who have shown that repeats of acidic residues when polymerized by the ribosome, before the nascent peptide fills the NPET, can induce Intrinsic Ribosome Destabilization (IRD) in prokaryotes^{2,3} and eukaryotes¹. They showed that the effect of the acidic residues depends on the bulkiness of the nascent chain². In our case, even if the nature of the nascent chain is clearly important (*i.e.* not all the proteins with proximal acidic residues are EttA-dependent for their expression) there is no relation with the size of the aa of the nascent chain (**Fig. 2a**). In our case, the effect is most likely dependent on the conformation of the nascent chain within the exit tunnel of the ribosome.

ARE ABC-F proteins provide resistance against antibiotics that target the PTC and the NPET^{10,14-20} and most of these antibiotics are context dependent^{4,5,73,74} (*i.e.* the sequence of the nascent peptide is important for the action of the antibiotic). Thus, in this condition also, the aa sequence in the NPET has an importance and therefore the mechanism has some similarity with what we present here, despite the absence of an inducer (antibiotic) in the case of EttA. This suggests that the action of ARE ABC-F and ABC-F on the ribosome are similar and have evolved from a general rescue mechanism.

Regarding EttA's cellular role, our study highlights its direct influence on three genes (*aceB*, *frdD*, and *fumC*), along with an indirect impact on *aceA*. These genes are functionally interconnected within the TCA and glyoxylate shunt pathways (**Fig. 1a**). This suggests EttA's ability to govern the expression of functionally related genes, emphasizing its role in coordinating key metabolic pathways. For the other EttA-dependent genes, some functionally related links can also be seen. The protein/nucleic acid deglycase 1 (HchA) repairs glyoxal- and methylglyoxal-glycated proteins^{75,76} as well as nucleotides^{27,28} by releasing glycolate or lactate from the modified amino acid or nucleotide. The glycolate can be converted into glyoxylate by the Glycolate dehydrogenase (GlcDEF)⁷⁷ and will benefit from the EttA-dependent expression of *aceB* for its degradation. The function of the protein YjbJ is unknown, but its expression is abundant during the stationary phase and salt stress^{78,79} as is the membrane protein, ElaB, which has been associated with resistance to multiple stresses⁸⁰. MgtA is an ATP-dependent Mg²⁺ importer⁶⁶ expressed when cells are deprived of Mg²⁺. The regulation of its expression by EttA through the leader peptide MgtL presumably helps the cells to regulate Mg²⁺ homeostasis. The last identified EttA target is the protein RraB, an inhibitor of the hydrolase activity of RNase E⁸¹⁻⁸³, the main RNase of *E. coli*⁸⁴. RraB binds to RNase E and modulates its activity towards specific mRNA targets⁸², that can be another level of regulation mediated by EttA. These results suggest that EttA can be a regulator of central metabolism and beyond. Moreover, replacement of the acidic residues in the construct AceB-NQ maintains the function of the enzyme and makes its expression EttA independent (**Fig. 3a and Extended Data Fig. 5a**) showing that the acidic residues are not essential for the function of AceB so that they can be used as a regulatory signal. A role in the regulation of gene expression was also proposed for the ARE-ABC-F LmrC¹⁸. Here, we have demonstrated that EttA exerts control over protein expression through two distinct mechanisms: a direct influence on the early stages of elongation and its interaction with leader peptides. Notably, our findings elucidate EttA's involvement in a regulatory network that enhances the expression of *mgtA*, particularly when integrated with the transcriptional regulation mediated by the *mgtL* leader peptide. These observations underscore the pivotal role of EttA within the cellular stress response system. It is

moreover induced by high salt (**Fig. 1b**), annotated as part of the RpoS regulon^{85,86} and regulates other genes induced by stress and salt. . In our previous study ^{6,7}, we unveiled a dependency of ETTA's influence on peptide bond formation upon the ADP:ATP ratio. Although its primary impact was observed during the initial peptide formation, these findings underscore ETTA's capacity to discern alterations in the ADP:ATP ratio. Significantly, our discovery that ETTA predominantly governs the expression of genes intricately involved in central metabolism, which in turn regulate cellular energy levels, suggest that ETTA possesses the ability to modulate their expression in accordance with the prevailing cellular energy.

Our results demonstrate that a fine tuning of protein synthesis at the translation level (30 to 50% change) can have a dramatic impact on bacteria physiology. Indeed, ETTA plays a key role in the regulation of the interconnection of the TCA and glyoxylate shunt pathways through the regulation at the translation level of *aceB*, *fumC* and *frdD* genes. The reduced expression of those genes principally *aceB* and indirectly *aceA* in the $\Delta ettA$ strain, induces different growth phenotypes by reducing the glyoxylate shunt metabolic flux in favor of the TCA cycle or the tartronate-semialdehyde flux. The $\Delta ettA$ strain grows better on a medium where glyoxylate is the only carbon source but worse on a medium where aa are the only carbon source and when cells are stressed by salt (**Fig. 1a, c**). The WT strain in the MMAA NaCl medium manages the salt stress by funneling the metabolic flux through the glyoxylate and the tartronate-semialdehyde pathways (**Fig. 3c**), which should have two advantages: an increase of metabolic flux towards glycolysis to generate osmoprotectants like sucrose⁸⁷ and trehalose⁸⁸ and a reduction in the flux to the bottom part of the TCA and therefore reducing the production of NADH and NADPH. These results support recent studies that have shown the importance of the glyoxylate shunt in stress conditions^{64,65,89-91}. The previously established dependence of ETTA's activity on ADP:ATP ratio provides a direct mechanism to connect its regulatory effects to cellular energy status, a topic that should be the focus of future studies.

ACKNOWLEDGEMENTS

FO, TO and GB were supported by funds from the CNRS (UMR8261), Université Paris Cité, the LABEX program (DYNAMO ANR-11-LABX-0011), and two ANR grants (EZOtrad/ANR-14-ACHN-0027 and ABC-F_AB/ANR-18-CE35-0010). FO received a fellowship from the Edmond de Rothschild Foundation. This work was also supported by the EQUIPEX CACSICE (ANR-11-EQPX-0008), through funding of the Proteomic Platform of IBPC. We express our great gratitude to Pr. Hirotada Mori for his gifts of the Keio collection and the YFP fusion strains collection. We thank Alexandre Pozza for its help with SEC-MALS experiments. The authors thank Jackie Plumbridge, Nicolas Biais and John F. Hunt for their advice and help.

AUTHOR CONTRIBUTIONS

FO constructed all the strains, performed most of the experiments and prepared the figures, TO and SN performed some bacterial cultures and samples preparations, SN performed the northern-blot experiments, MH performed the proteomic analysis, AON generated early results used for this study. FO, GB and LM analyzed the data, GB designed the research program. GB, LM and FO wrote the manuscript in consultation with the other authors.

COMPETING FINANCIAL INTERESTS

The authors declare no competing financial interests.

REFERENCES

- 1 Ito, Y. *et al.* Nascent peptide-induced translation discontinuation in eukaryotes impacts biased amino acid usage in proteomes. *Nat Commun* **13**, 7451 (2022). <https://doi.org/10.1038/s41467-022-35156-x>
- 2 Chadani, Y. *et al.* Nascent polypeptide within the exit tunnel stabilizes the ribosome to counteract risky translation. *EMBO J* **40**, e108299 (2021). <https://doi.org/10.15252/embj.2021108299>
- 3 Chadani, Y. *et al.* Intrinsic Ribosome Destabilization Underlies Translation and Provides an Organism with a Strategy of Environmental Sensing. *Mol Cell* **68**, 528-539 e525 (2017). <https://doi.org/10.1016/j.molcel.2017.10.020>
- 4 Marks, J. *et al.* Context-specific inhibition of translation by ribosomal antibiotics targeting the peptidyl transferase center. *Proc Natl Acad Sci U S A* **113**, 12150-12155 (2016). <https://doi.org/10.1073/pnas.1613055113>
- 5 Choi, J. *et al.* Dynamics of the context-specific translation arrest by chloramphenicol and linezolid. *Nature chemical biology* **16**, 310-317 (2020). <https://doi.org/10.1038/s41589-019-0423-2>
- 6 Boel, G. *et al.* The ABC-F protein EttA gates ribosome entry into the translation elongation cycle. *Nat Struct Mol Biol* **21**, 143-151 (2014). <https://doi.org/10.1038/nsmb.2740>
- 7 Chen, B. *et al.* EttA regulates translation by binding the ribosomal E site and restricting ribosome-tRNA dynamics. *Nat Struct Mol Biol* **21**, 152-159 (2014). <https://doi.org/10.1038/nsmb.2741>
- 8 Davidson, A. L., Dassa, E., Orelle, C. & Chen, J. Structure, function, and evolution of bacterial ATP-binding cassette systems. *Microbiology and molecular biology reviews : MMBR* **72**, 317-364, table of contents (2008). <https://doi.org/10.1128/MMBR.00031-07>
- 9 Sharkey, L. K., Edwards, T. A. & O'Neill, A. J. ABC-F Proteins Mediate Antibiotic Resistance through Ribosomal Protection. *mBio* **7**, e01975 (2016). <https://doi.org/10.1128/mBio.01975-15>
- 10 Crowe-McAuliffe, C. *et al.* Structural basis for antibiotic resistance mediated by the *Bacillus subtilis* ABCF ATPase VmlR. *Proc Natl Acad Sci U S A* **115**, 8978-8983 (2018). <https://doi.org/10.1073/pnas.1808535115>
- 11 Murina, V., Kasari, M., Hauryliuk, V. & Atkinson, G. C. Antibiotic resistance ABCF proteins reset the peptidyl transferase centre of the ribosome to counter translational arrest. *Nucleic Acids Res* **46**, 3753-3763 (2018). <https://doi.org/10.1093/nar/gky050>
- 12 Su, W. *et al.* Ribosome protection by antibiotic resistance ATP-binding cassette protein. *Proc Natl Acad Sci U S A* **115**, 5157-5162 (2018). <https://doi.org/10.1073/pnas.1803313115>
- 13 Murina, V. *et al.* ABCF ATPases Involved in Protein Synthesis, Ribosome Assembly and Antibiotic Resistance: Structural and Functional Diversification across the Tree of Life. *J Mol Biol* **431**, 3568-3590 (2019). <https://doi.org/10.1016/j.jmb.2018.12.013>
- 14 Lenart, J., Vimberg, V., Vesela, L., Janata, J. & Balikova Novotna, G. Detailed mutational analysis of Vga(A) interdomain linker: implication for antibiotic resistance specificity and mechanism. *Antimicrob Agents Chemother* **59**, 1360-1364 (2015). <https://doi.org/10.1128/AAC.04468-14>
- 15 Vimberg, V. *et al.* Ribosome-Mediated Attenuation of vga(A) Expression Is Shaped by the Antibiotic Resistance Specificity of Vga(A) Protein Variants. *Antimicrob Agents Chemother* **64** (2020). <https://doi.org/10.1128/AAC.00666-20>

- 16 Obana, N. *et al.* Genome-encoded ABCF factors implicated in intrinsic antibiotic resistance in Gram-positive bacteria: VmlR2, Ard1 and CplR. *Nucleic Acids Res* **51**, 4536-4554 (2023). <https://doi.org:10.1093/nar/gkad193>
- 17 Mohamad, M. *et al.* Sal-type ABC-F proteins: intrinsic and common mediators of pleuromutilin resistance by target protection in staphylococci. *Nucleic Acids Res* **50**, 2128-2142 (2022). <https://doi.org:10.1093/nar/gkac058>
- 18 Koberska, M. *et al.* Beyond Self-Resistance: ABCF ATPase LmrC Is a Signal-Transducing Component of an Antibiotic-Driven Signaling Cascade Accelerating the Onset of Lincomycin Biosynthesis. *mBio* **12**, e0173121 (2021). <https://doi.org:10.1128/mBio.01731-21>
- 19 Crowe-McAuliffe, C. *et al.* Structural basis of ABCF-mediated resistance to pleuromutilin, lincosamide, and streptogramin A antibiotics in Gram-positive pathogens. *Nat Commun* **12**, 3577 (2021). <https://doi.org:10.1038/s41467-021-23753-1>
- 20 Crowe-McAuliffe, C. *et al.* Structural basis for PoxTA-mediated resistance to phenicol and oxazolidinone antibiotics. *Nat Commun* **13**, 1860 (2022). <https://doi.org:10.1038/s41467-022-29274-9>
- 21 Ousalem, F., Singh, S., Chesneau, O., Hunt, J. F. & Boel, G. ABC-F proteins in mRNA translation and antibiotic resistance. *Research in microbiology* **170**, 435-447 (2019). <https://doi.org:10.1016/j.resmic.2019.09.005>
- 22 Ousalem, F. *et al.* Comparative genetic, biochemical, and biophysical analyses of the four *E. coli* ABCF paralogs support distinct functions related to mRNA translation. *bioRxiv*, 2023.2006.2011.543863 (2023). <https://doi.org:10.1101/2023.06.11.543863>
- 23 Singh, S. *et al.* Cryo-EM studies of the four *E. coli* paralogs establish ABCF proteins as master plumbers of the peptidyl-transferase center of the ribosome. *bioRxiv*, 2023.2006.2015.543498 (2023). <https://doi.org:10.1101/2023.06.15.543498>
- 24 Fostier, C. R. *et al.* ABC-F translation factors: from antibiotic resistance to immune response. *FEBS Lett* **595**, 675-706 (2021). <https://doi.org:10.1002/1873-3468.13984>
- 25 Punta, M. *et al.* The Pfam protein families database. *Nucleic Acids Res* **40**, D290-301 (2012). <https://doi.org:10.1093/nar/gkr1065>
- 26 Smith, P. C. *et al.* ATP binding to the motor domain from an ABC transporter drives formation of a nucleotide sandwich dimer. *Mol Cell* **10**, 139-149 (2002). [https://doi.org:10.1016/s1097-2765\(02\)00576-2](https://doi.org:10.1016/s1097-2765(02)00576-2)
- 27 Cui, Z. *et al.* Interplay between an ATP-binding cassette F protein and the ribosome from *Mycobacterium tuberculosis*. *Nat Commun* **13**, 432 (2022). <https://doi.org:10.1038/s41467-022-28078-1>
- 28 Su, T. *et al.* Structure and function of Vms1 and Arb1 in RQC and mitochondrial proteome homeostasis. *Nature* **570**, 538-542 (2019). <https://doi.org:10.1038/s41586-019-1307-z>
- 29 Doerfel, L. K. *et al.* EF-P is essential for rapid synthesis of proteins containing consecutive proline residues. *Science* **339**, 85-88 (2013). <https://doi.org:10.1126/science.1229017>
- 30 Ude, S. *et al.* Translation elongation factor EF-P alleviates ribosome stalling at polyproline stretches. *Science* **339**, 82-85 (2013). <https://doi.org:10.1126/science.1228985>
- 31 Gutierrez, E. *et al.* eIF5A promotes translation of polyproline motifs. *Mol Cell* **51**, 35-45 (2013). <https://doi.org:10.1016/j.molcel.2013.04.021>

- 32 Murina, V., Kasari, M., Hauryliuk, V. & Atkinson, G. C. Antibiotic resistance ABCF proteins reset the peptidyl transferase centre of the ribosome to counter translational arrest. *Nucleic Acids Res*, gky050-gky050 (2018). <https://doi.org:10.1093/nar/gky050>
- 33 Fostier, C. R. *et al.* Regulation of the macrolide resistance ABC-F translation factor MsrD. *Nature Communications* **14**, 3891 (2023). <https://doi.org:10.1038/s41467-023-39553-8>
- 34 Vazquez de Aldana, C. R., Marton, M. J. & Hinnebusch, A. G. GCN20, a novel ATP binding cassette protein, and GCN1 reside in a complex that mediates activation of the eIF-2 alpha kinase GCN2 in amino acid-starved cells. *The EMBO journal* **14**, 3184-3199 (1995).
- 35 Sattlegger, E. & Hinnebusch, A. G. Polyribosome binding by GCN1 is required for full activation of eukaryotic translation initiation factor 2{alpha} kinase GCN2 during amino acid starvation. *J Biol Chem* **280**, 16514-16521 (2005). <https://doi.org:10.1074/jbc.M414566200>
- 36 Dong, J., Lai, R., Jennings, J. L., Link, A. J. & Hinnebusch, A. G. The novel ATP-binding cassette protein ARB1 is a shuttling factor that stimulates 40S and 60S ribosome biogenesis. *Mol Cell Biol* **25**, 9859-9873 (2005). <https://doi.org:10.1128/MCB.25.22.9859-9873.2005>
- 37 Paytubi, S. *et al.* ABC50 promotes translation initiation in mammalian cells. *J Biol Chem* **284**, 24061-24073 (2009). <https://doi.org:10.1074/jbc.M109.031625>
- 38 Arora, H. *et al.* The ATP-Binding Cassette Gene ABCF1 Functions as an E2 Ubiquitin-Conjugating Enzyme Controlling Macrophage Polarization to Dampen Lethal Septic Shock. *Immunity* **50**, 418-431 e416 (2019). <https://doi.org:10.1016/j.immuni.2019.01.014>
- 39 Richard, M., Drouin, R. & Beaulieu, A. D. ABC50, a novel human ATP-binding cassette protein found in tumor necrosis factor-alpha-stimulated synoviocytes. *Genomics* **53**, 137-145 (1998). <https://doi.org:10.1006/geno.1998.5480>
- 40 Semov, A. *et al.* Alterations in TNF- and IL-related gene expression in space-flown WI38 human fibroblasts. *FASEB J* **16**, 899-901 (2002). <https://doi.org:10.1096/fj.01-1002fje>
- 41 Yu, Y., Zhang, Y., Zhu, Z. & Berger, S. A. ABC50 modulates sensitivity of HL60 leukemic cells to endoplasmic reticulum (ER) stress-induced cell death. *Biochem Pharmacol* **81**, 488-497 (2011). <https://doi.org:10.1016/j.bcp.2010.11.007>
- 42 Setia, N., Abbas, O., Sousa, Y., Garb, J. L. & Mahalingam, M. Profiling of ABC transporters ABCB5, ABCF2 and nestin-positive stem cells in nevi, in situ and invasive melanoma. *Modern pathology : an official journal of the United States and Canadian Academy of Pathology, Inc* **25**, 1169-1175 (2012). <https://doi.org:10.1038/modpathol.2012.71>
- 43 Verma, N., Ahuja, V. & Paul, J. Profiling of ABC transporters during active ulcerative colitis and in vitro effect of inflammatory modulators. *Digestive diseases and sciences* **58**, 2282-2292 (2013). <https://doi.org:10.1007/s10620-013-2636-7>
- 44 Lee, M. N. *et al.* Identification of regulators of the innate immune response to cytosolic DNA and retroviral infection by an integrative approach. *Nat Immunol* **14**, 179-185 (2013). <https://doi.org:10.1038/ni.2509>
- 45 Boonstra, R. *et al.* Mitoxantrone resistance in a small cell lung cancer cell line is associated with ABCA2 upregulation. *British journal of cancer* **90**, 2411-2417 (2004). <https://doi.org:10.1038/sj.bjc.6601863>
- 46 Ogawa, Y. *et al.* Clinical role of ABCF2 expression in breast cancer. *Anticancer research* **26**, 1809-1814 (2006).

- 47 Hendig, D. *et al.* Characterization of the ATP-binding cassette transporter gene expression profile in Y79: a retinoblastoma cell line. *Mol Cell Biochem* **328**, 85-92 (2009). <https://doi.org/10.1007/s11010-009-0077-6>
- 48 Cunha, I. W. *et al.* Identification of genes associated with local aggressiveness and metastatic behavior in soft tissue tumors. *Transl Oncol* **3**, 23-32 (2010). <https://doi.org/10.1593/tlo.09166>
- 49 Hlavata, I. *et al.* The role of ABC transporters in progression and clinical outcome of colorectal cancer. *Mutagenesis* **27**, 187-196 (2012). <https://doi.org/10.1093/mutage/ger075>
- 50 Hlavac, V. *et al.* The expression profile of ATP-binding cassette transporter genes in breast carcinoma. *Pharmacogenomics* **14**, 515-529 (2013). <https://doi.org/10.2217/pgs.13.26>
- 51 Antonova, O. *et al.* Changes in the gene expression profile of the bladder cancer cell lines after treatment with Helix lucorum and Rapana venosa hemocyanin. *J BUON* **20**, 180-187 (2015).
- 52 Li, X. *et al.* Elevated microRNA-23a Expression Enhances the Chemoresistance of Colorectal Cancer Cells with Microsatellite Instability to 5-Fluorouracil by Directly Targeting ABCF1. *Curr Protein Pept Sci* **16**, 301-309 (2015). <https://doi.org/10.2174/138920371604150429153309>
- 53 Boel, G. *et al.* Codon influence on protein expression in E. coli correlates with mRNA levels. *Nature* **529**, 358-363 (2016). <https://doi.org/10.1038/nature16509>
- 54 Presnyak, V. *et al.* Codon optimality is a major determinant of mRNA stability. *Cell* **160**, 1111-1124 (2015). <https://doi.org/10.1016/j.cell.2015.02.029>
- 55 Bazzini, A. A. *et al.* Codon identity regulates mRNA stability and translation efficiency during the maternal-to-zygotic transition. *EMBO J* **35**, 2087-2103 (2016). <https://doi.org/10.15252/embj.201694699>
- 56 Mishima, Y. & Tomari, Y. Codon Usage and 3' UTR Length Determine Maternal mRNA Stability in Zebrafish. *Mol Cell* **61**, 874-885 (2016). <https://doi.org/10.1016/j.molcel.2016.02.027>
- 57 Zampieri, M., Horl, M., Hotz, F., Muller, N. F. & Sauer, U. Regulatory mechanisms underlying coordination of amino acid and glucose catabolism in Escherichia coli. *Nat Commun* **10**, 3354 (2019). <https://doi.org/10.1038/s41467-019-11331-5>
- 58 Kaplun, A. *et al.* Glyoxylate carboligase lacks the canonical active site glutamate of thiamine-dependent enzymes. *Nature chemical biology* **4**, 113-118 (2008). <https://doi.org/10.1038/nchembio.62>
- 59 Gupta, N. K. & Vennessland, B. Glyoxylate Carboligase of Escherichia Coli: A Flavoprotein. *The Journal of biological chemistry* **239**, 3787-3789 (1964).
- 60 Chang, Y. Y., Wang, A. Y. & Cronan, J. E., Jr. Molecular cloning, DNA sequencing, and biochemical analyses of Escherichia coli glyoxylate carboligase. An enzyme of the acetohydroxy acid synthase-pyruvate oxidase family. *The Journal of biological chemistry* **268**, 3911-3919 (1993).
- 61 Ornston, L. N. & Ornston, M. K. Regulation of glyoxylate metabolism in Escherichia coli K-12. *Journal of bacteriology* **98**, 1098-1108 (1969). <https://doi.org/10.1128/jb.98.3.1098-1108.1969>
- 62 Karp, P. D. *et al.* The EcoCyc Database. *EcoSal Plus* **8** (2018). <https://doi.org/10.1128/ecosalplus.ESP-0006-2018>
- 63 Zelcbuch, L. *et al.* An in vivo metabolic approach for deciphering the product specificity of glycerate kinase proves that both E. coli's glycerate kinases generate 2-phosphoglycerate. *PloS one* **10**, e0122957 (2015). <https://doi.org/10.1371/journal.pone.0122957>

- 64 Erkut, C., Gade, V. R., Laxman, S. & Kurzchalia, T. V. The glyoxylate shunt is essential for desiccation tolerance in *C. elegans* and budding yeast. *Elife* **5**, e13614 (2016). <https://doi.org:10.7554/eLife.13614>
- 65 Yuenyong, W., Sirikantaramas, S., Qu, L. J. & Buaboocha, T. Isocitrate lyase plays important roles in plant salt tolerance. *BMC Plant Biol* **19**, 472 (2019). <https://doi.org:10.1186/s12870-019-2086-2>
- 66 Smith, R. L. & Maguire, M. E. Microbial magnesium transport: unusual transporters searching for identity. *Mol Microbiol* **28**, 217-226 (1998). <https://doi.org:10.1046/j.1365-2958.1998.00810.x>
- 67 Zhao, G., Kong, W., Weatherspoon-Griffin, N., Clark-Curtiss, J. & Shi, Y. Mg²⁺ facilitates leader peptide translation to induce riboswitch-mediated transcription termination. *EMBO J* **30**, 1485-1496 (2011). <https://doi.org:10.1038/emboj.2011.66>
- 68 Gall, A. R. *et al.* Mg²⁺ regulates transcription of *mgtA* in *Salmonella Typhimurium* via translation of proline codons during synthesis of the MgtL peptide. *Proc Natl Acad Sci U S A* **113**, 15096-15101 (2016). <https://doi.org:10.1073/pnas.1612268113>
- 69 Glick, B. R. & Ganoza, M. C. Identification of a soluble protein that stimulates peptide bond synthesis. *Proc Natl Acad Sci U S A* **72**, 4257-4260 (1975). <https://doi.org:10.1073/pnas.72.11.4257>
- 70 Huter, P. *et al.* Structural Basis for Polyproline-Mediated Ribosome Stalling and Rescue by the Translation Elongation Factor EF-P. *Mol Cell* **68**, 515-527 e516 (2017). <https://doi.org:10.1016/j.molcel.2017.10.014>
- 71 Woolstenhulme, C. J., Guydosh, N. R., Green, R. & Buskirk, A. R. High-precision analysis of translational pausing by ribosome profiling in bacteria lacking EFP. *Cell Rep* **11**, 13-21 (2015). <https://doi.org:10.1016/j.celrep.2015.03.014>
- 72 Starosta, A. L. *et al.* Translational stalling at polyproline stretches is modulated by the sequence context upstream of the stall site. *Nucleic Acids Res* **42**, 10711-10719 (2014). <https://doi.org:10.1093/nar/gku768>
- 73 Beckert, B. *et al.* Structural and mechanistic basis for translation inhibition by macrolide and ketolide antibiotics. *Nat Commun* **12**, 4466 (2021). <https://doi.org:10.1038/s41467-021-24674-9>
- 74 Kannan, K. *et al.* The general mode of translation inhibition by macrolide antibiotics. *Proc Natl Acad Sci U S A* **111**, 15958-15963 (2014). <https://doi.org:10.1073/pnas.1417334111>
- 75 Richarme, G. *et al.* Guanine glycation repair by DJ-1/Park7 and its bacterial homologs. *Science* **357**, 208-211 (2017). <https://doi.org:10.1126/science.aag1095>
- 76 Richarme, G. *et al.* Parkinsonism-associated protein DJ-1/Park7 is a major protein deglycase that repairs methylglyoxal- and glyoxal-glycated cysteine, arginine, and lysine residues. *The Journal of biological chemistry* **290**, 1885-1897 (2015). <https://doi.org:10.1074/jbc.M114.597815>
- 77 Pellicer, M. T., Badia, J., Aguilar, J. & Baldoma, L. *glc* locus of *Escherichia coli*: characterization of genes encoding the subunits of glycolate oxidase and the *glc* regulator protein. *Journal of bacteriology* **178**, 2051-2059 (1996). <https://doi.org:10.1128/jb.178.7.2051-2059.1996>
- 78 Weber, H., Polen, T., Heuveling, J., Wendisch, V. F. & Hengge, R. Genome-wide analysis of the general stress response network in *Escherichia coli*: sigma^S-dependent genes, promoters, and sigma factor selectivity. *Journal of bacteriology* **187**, 1591-1603 (2005). <https://doi.org:10.1128/JB.187.5.1591-1603.2005>

- 79 Weber, A., Kogl, S. A. & Jung, K. Time-dependent proteome alterations under osmotic stress during aerobic and anaerobic growth in *Escherichia coli*. *Journal of bacteriology* **188**, 7165-7175 (2006). <https://doi.org:10.1128/JB.00508-06>
- 80 Guo, Y. *et al.* Tail-Anchored Inner Membrane Protein ElaB Increases Resistance to Stress While Reducing Persistence in *Escherichia coli*. *Journal of bacteriology* **199** (2017). <https://doi.org:10.1128/JB.00057-17>
- 81 Lee, K. *et al.* RraA. *Cell* **114**, 623-634 (2003). <https://doi.org:10.1016/j.cell.2003.08.003>
- 82 Gao, J. *et al.* Differential modulation of *E. coli* mRNA abundance by inhibitory proteins that alter the composition of the degradosome. *Mol Microbiol* **61**, 394-406 (2006). <https://doi.org:10.1111/j.1365-2958.2006.05246.x>
- 83 Yeom, J. H. *et al.* Inhibitory effects of RraA and RraB on RNase E-related enzymes imply conserved functions in the regulated enzymatic cleavage of RNA. *FEMS Microbiol Lett* **285**, 10-15 (2008). <https://doi.org:10.1111/j.1574-6968.2008.01205.x>
- 84 Carpousis, A. J. The RNA degradosome of *Escherichia coli*: an mRNA-degrading machine assembled on RNase E. *Annu Rev Microbiol* **61**, 71-87 (2007). <https://doi.org:10.1146/annurev.micro.61.080706.093440>
- 85 Huerta, A. M. & Collado-Vides, J. Sigma70 promoters in *Escherichia coli*: specific transcription in dense regions of overlapping promoter-like signals. *J Mol Biol* **333**, 261-278 (2003). <https://doi.org:10.1016/j.jmb.2003.07.017>
- 86 Keseler, I. M. *et al.* The EcoCyc Database in 2021. *Front Microbiol* **12**, 711077 (2021). <https://doi.org:10.3389/fmicb.2021.711077>
- 87 Gouffi, K. *et al.* Sucrose is a nonaccumulated osmoprotectant in *Sinorhizobium meliloti*. *Journal of bacteriology* **180**, 5044-5051 (1998). <https://doi.org:10.1128/JB.180.19.5044-5051.1998>
- 88 Cayley, S. & Record, M. T., Jr. Roles of cytoplasmic osmolytes, water, and crowding in the response of *Escherichia coli* to osmotic stress: biophysical basis of osmoprotection by glycine betaine. *Biochemistry* **42**, 12596-12609 (2003). <https://doi.org:10.1021/bi0347297>
- 89 Ahn, S., Jung, J., Jang, I. A., Madsen, E. L. & Park, W. Role of Glyoxylate Shunt in Oxidative Stress Response. *The Journal of biological chemistry* **291**, 11928-11938 (2016). <https://doi.org:10.1074/jbc.M115.708149>
- 90 Park, C., Shin, B. & Park, W. Alternative fate of glyoxylate during acetate and hexadecane metabolism in *Acinetobacter oleivorans* DR1. *Sci Rep* **9**, 14402 (2019). <https://doi.org:10.1038/s41598-019-50852-3>
- 91 Koedooder, C. *et al.* The Role of the Glyoxylate Shunt in the Acclimation to Iron Limitation in Marine Heterotrophic Bacteria. *Frontiers in Marine Science* **5** (2018). <https://doi.org:10.3389/fmars.2018.00435>
- 92 Blattner, F. R. *et al.* The Complete Genome Sequence of *Escherichia coli* K-12. *Science* **277**, 1453-1462 (1997). <https://doi.org:doi:10.1126/science.277.5331.1453>
- 93 St-Pierre, F. *et al.* One-step cloning and chromosomal integration of DNA. *ACS synthetic biology* **2**, 537-541 (2013). <https://doi.org:10.1021/sb400021j>
- 94 Otsuka, Y. *et al.* GenoBase: comprehensive resource database of *Escherichia coli* K-12. *Nucleic Acids Res* **43**, D606-617 (2015). <https://doi.org:10.1093/nar/gku1164>

- 95 Datsenko, K. A. & Wanner, B. L. One-step inactivation of chromosomal genes in *Escherichia coli* K-12 using PCR products. *Proc Natl Acad Sci U S A* **97**, 6640-6645 (2000). <https://doi.org:10.1073/pnas.120163297>
- 96 Baba, T. *et al.* Construction of *Escherichia coli* K-12 in-frame, single-gene knockout mutants: the Keio collection. *Molecular systems biology* **2**, 2006 0008 (2006). <https://doi.org:10.1038/msb4100050>
- 97 Jansson, M. *et al.* High-level production of uniformly (1)(5)N- and (1)(3)C-enriched fusion proteins in *Escherichia coli*. *Journal of biomolecular NMR* **7**, 131-141 (1996).
- 98 Stead, M. B. *et al.* RNA snap™: a rapid, quantitative and inexpensive, method for isolating total RNA from bacteria. *Nucleic Acids Research* **40**, e156-e156 (2012). <https://doi.org:10.1093/nar/gks680>
- 99 Langmead, B. & Salzberg, S. L. Fast gapped-read alignment with Bowtie 2. *Nature methods* **9**, 357-359 (2012). <https://doi.org:10.1038/nmeth.1923>
- 100 Ramirez-Gonzalez, R. H., Bonnal, R., Caccamo, M. & Maclean, D. Bio-samtools: Ruby bindings for SAMtools, a library for accessing BAM files containing high-throughput sequence alignments. *Source code for biology and medicine* **7**, 6 (2012). <https://doi.org:10.1186/1751-0473-7-6>
- 101 Liao, Y., Smyth, G. K. & Shi, W. featureCounts: an efficient general purpose program for assigning sequence reads to genomic features. *Bioinformatics (Oxford, England)* **30**, 923-930 (2014). <https://doi.org:10.1093/bioinformatics/btt656>
- 102 Team, R. C. R: A language and environment for statistical computing. <http://www.r-project.org/> (2012).
- 103 Anders, S. & Huber, W. Differential expression analysis for sequence count data. *Genome Biology* **11**, R106 (2010). <https://doi.org:10.1186/gb-2010-11-10-r106>
- 104 Tyanova, S., Temu, T. & Cox, J. The MaxQuant computational platform for mass spectrometry-based shotgun proteomics. *Nat Protoc* **11**, 2301-2319 (2016). <https://doi.org:10.1038/nprot.2016.136>
- 105 Cox, J. *et al.* Accurate proteome-wide label-free quantification by delayed normalization and maximal peptide ratio extraction, termed MaxLFQ. *Mol Cell Proteomics* **13**, 2513-2526 (2014). <https://doi.org:10.1074/mcp.M113.031591>
- 106 Vazquez-Laslop, N., Thum, C. & Mankin, A. S. Molecular mechanism of drug-dependent ribosome stalling. *Mol Cell* **30**, 190-202 (2008). <https://doi.org:10.1016/j.molcel.2008.02.026>
- 107 Keseler, I. M. *et al.* The EcoCyc database: reflecting new knowledge about *Escherichia coli* K-12. *Nucleic Acids Research* **45**, D543-D550 (2016). <https://doi.org:10.1093/nar/gkw1003>

FIGURE LEGENDS

Fig. 1: Loss of EttA impacts the TCA and glyoxylate shunt pathways and stress genes. **a**, Growth curves of the WT, $\Delta ettA$ and C_{ettA} strains in MMAA medium without or with NaCl (0.2 and 0.4 M). Error bars represent mean \pm standard deviation (s.d.) for triplicate experiments. Above and below the curves, heatmaps showing the absorbance (OD_{600}) of cultures at various phases of the growth of the WT strain (t_0 to t_4). The dotted lines indicate the OD values assigned to the heatmap. Right: Table representing the difference in lag phase of $\Delta ettA$ versus WT and C_{ettA} strains and their respective doubling times in the same media calculated as described in the methods. **b**, Graph showing the fluorescence intensity at $OD_{600}=1.4$ of the MG1655 $ettA:yfp$ strain expressing $ettA$ in a translational fusion with a yfp gene, in the MMAA medium at different NaCl concentrations (0, 0.2, 0.3, 0.4 or 0.5 M). Background fluorescence of a culture without YFP has been subtracted, the error bars represent mean \pm s.d. for triplicate experiments. **c**, Representation of TCA cycle and the glyoxylate shunt pathways showing intermediary products (in boxes), genes coding the enzymes (next to the reaction arrows) and cofactors (in grey). Genes in red were identified in the proteomic study as less expressed in the $\Delta ettA$ strain (**Extended Data Fig. 1d**). Grey heatmaps show the absorbance (OD_{600}) of cultures of WT, $\Delta ettA$ and C_{ettA} strains, at the same growth staged as panel (a), for cultures on different carbon sources at a concentration of 0.3 M (malate, fumarate and succinate) or 0.15 M (glyoxylate) in the MMAA medium. Heatmaps in green show the YFP fluorescence level of the same three strains with a yfp translational fusion inserted in the genome in frame with the $aceB$, $aceA$, $fumC$, $yjbJ$ and $hchA$ genes ($aceB:yfp$, $aceA:yfp$, $fumC:yfp$, $yjbJ:yfp$ and $hchA:yfp$) grown in MMAA medium or LB medium for $fumC:yfp$. Scales are presented on the top of each heatmap. Full growth curves are presented in the **Extended Data Fig. 1i**.

Fig. 2: EttA assists ribosomes during the synthesis of peptides with repeated acidic residues.

a, The beginning of the coding sequences of the $aceB$ (malate synthase), $aceA$ (isocitrate lyase), $fumC$ (fumarase C), $yjbJ$ (putative stress response protein), $hchA$ (protein/nucleic acid deglycase 1), $frdD$ (fumarate reductase subunit D), $elaB$ (tail-anchored inner membrane protein) and $rraB$ (ribonuclease E inhibitor protein B) genes were cloned in a low-copy plasmid (pMMB) under the control of an IPTG inducible promoter and translationally fused to a yfp gene. The corresponding aa sequence is presented on the left side. Point mutations tested (dark green) of the acidic residues (purple) responsible for the EttA-dependent expression are indicated in the sequence, other mutations upstream of the acidic residues were also tested for $aceB$ and $yjbJ$. Two $aceA:yfp$ fusions were made, one with only the intergenic $aceB-A$ sequence and the second one with the operon sequence ($aceB$ gene and the intergenic region). Cultures were performed in LB_Amp100 medium in the presence of 1 mM IPTG, to avoid differential growth between the strains. Histograms show the ratios of YFP intensity in the $\Delta ettA$ vs. WT strain for the different constructs (details of the calculation of the ratio and propagation of the error is given in the methods section) for the different constructs. Ratios are measured at the end of growth. The growth curves, results for the complemented strain (C_{ettA}) and the details of the constructions are presented in **Extended Data Fig. 3**. **b**, Histograms showing the ratios of YFP intensity in the presence or absence of 5 μ M EttA after 150 min of *in vitro* translation (NEB PURExpress) of the different transcripts ($aceB_{1-10aa}:yfp$, $yjbJ_{1-5aa}:yfp$ and $rraB_{1-10aa}:yfp$) and for the same ones harboring the mutations that abolish EttA-dependency *in vivo*. *p* values of unpaired two-tailed *t*-tests are shown on the side of the bars (** ≤ 0.01 ; *** ≤ 0.001). **a and b**, Error bars represent mean \pm s.d. for triplicate experiments. **c**,

Toeprinting assay using *aceB*_{1-10aa} and *aceB*-NQ mRNA with or without His₆-EttA or His₆-EttA-EQ₂ at 5 μM. The position of ribosomes stalling at the initiation codon was verified by the addition of Thiostrepton and Retapamulin. **d**, Toeprinting assay of *yjbJ*_{1-5aa} and *yjbJ*-NQ mRNA with or without EttA or EttA-EQ₂ at 5 μM. **c and d**, the structure of the mRNA used for toeprinting is indicated above the gels. Empty and plain arrows indicate ribosomes blocked at the initiation or arrested on a specific motif during elongation, respectively.

Fig. 3: EttA-dependent synthesis of some proteins of the TCA/glyoxylate shunt pathways can explain the observed phenotypes of the Δ *ettA* strain. **a**, Representation of the TCA cycle, the glyoxylate shunt and the tartronate semialdehyde pathway showing intermediary products and genes encoding the enzymes. The expression of genes shown in red is dependent on EttA. Heatmaps show the OD₆₀₀ at various times of growth as in **Fig. 1a** from cultures in MM.Glyoxylate (purple frame) or MMAA 0.4 M NaCl (brown frame) media. The control experiments for the WT, Δ *ettA*, and *C_{ettA}* are presented on the top. The other heatmaps are for the same strains with a deletion of either *aceB*, *aceA*, *glcB*, *gcl*, *fumC*, *frdD* or *icd* gene (deletions are represented on the pathway map by red crosses) or for the same strains overexpressing *aceB* or *aceB*-NQ from a plasmid (\nearrow *aceB* and \nearrow *aceB*-NQ). For *aceA* overexpression (\nearrow *aceA*) from a plasmid, the three strains deleted of *aceA* were used. The OD equivalents of the heatmap color shadings are indicated above the control experiments (WT, Δ *ettA* and *C_{ettA}*) for the two tested media or above individual heatmaps if different. Growth curves are presented in **Extended Data Fig. 5**. **b and c**, Representation of the possible metabolic flux in MM.Glyoxylate medium (**b**) and MMAA 0.4 M NaCl medium (**c**) for the WT (blue) and Δ *ettA* (red) strains.

Fig. 4: Synthesis of the leader peptide MgtL by the ribosome is dependent on EttA. **a**, Model of the regulation of *mgtA* expression by Mg²⁺. At high intracellular Mg²⁺ concentrations, the translation of the entire leader peptide, MgtL, maintains the mRNA in a conformation where a Rho-dependent terminator (RDT) site is accessible for Rho to terminate the transcription of the mRNA. At low Mg²⁺ intracellular concentrations, dissociation of the elongating ribosome when polymerizing negatively charged residues of MgtL, changes the mRNA into a conformation where the RDT is no longer accessible, allowing the transcription of *mgtA*. **b**, Histograms showing the ratios of YFP fluorescence of Δ *ettA*/WT strains, for *mgtL*:yfp fusion (left), or *mgtL*_{1-5aa}:yfp fusion (right). Constructs express either the WT *mgtL* or a mutant (*mgtL*-QN) where two acidic residues (purple) were mutated (dark green). The constructions used are shown above the histograms and the sequence of MgtL is on the left. The YFP sequence used in this experiment contains a 6-residue N-terminal translation enhancer³³. The constructions were expressed from a pMMB plasmid and bacteria were grown in MMAA medium in the presence of Amp, 1 mM IPTG and 2 mM MgSO₄. Ratios are measured at the end of growth (see **Extended Data Fig. 6b**). **c**, Design of the mRNA used for IVTA. Histograms showing the ratios of YFP intensity with or without EttA (5 μM) after 150 min of *in vitro* translation of mRNA coding for WT or MgtL-QN YFP fusions. **b and c**, Error bars represent mean ± s.d. for triplicate experiments. Two-tailed *t*-tests was used to measure the *p* value (***) ≤ 0.001; ****) ≤ 0.0001). **d**, Toeprinting assay of *mgtL* and *mgtL*-NQ mRNA with or without His₆-EttA or His₆-EttA-EQ₂ at 5 μM. Empty and plain arrows indicate ribosomes blocked at the initiation or arrested on a specific motif during elongation, respectively.

Fig. 5: EttA rescues translation of mRNA encoding acidic residues at the beginning of translated sequences and shares a structural homology with EF-P. **a**, Histograms showing the ratio of the YFP fluorescence emission of $\Delta ettA$ /WT strains expressing the 5'UTR of *yjbJ* followed by a *yfp* gene where the exogenous coding sequence NKDEPD has been inserted after the initiating methionine using two different sets of synonymous codons (syn-codon, see methods). A similar construct with the 5'UTR of *aceB* is also presented as well as equivalent constructs where segments (10, 20, 30 or 40 aa) of the AceB-NQ sequence have been introduced between the initiating methionine and the NKDEPD sequence. Cartoons of the translated peptides in the exit tunnel of the ribosome are shown on the right. Results for the complemented strain (C_{ettA}) and the growth curves are presented in **Extended data Fig. 7a, b**. **b**, Histograms showing the ratio of YFP intensity after 150 min of *in vitro* translation of a UTR_{*aceB*}_MNKDEPD:*yfp* mRNA with or without EttA (5 μ M). Error bars represent the mean \pm s. d. for triplicate experiments. **c**, Violin plot showing the expression level of genes containing the ExD motif (- /X_{0,1}/ -) or not within the first 50 neo-synthesized aa by windows of 10 aa based on the log₂ $\Delta ettA$ /WT ratios obtained in the S₁₅ proteomic. The red and grey dotted lines represent the median and quartiles respectively. The *p* values are calculated using the Mann-Whitney test. The same analysis for the complemented strain (C_{ettA}) is presented in **Extended data Fig. 7d**. **d**, Model of EttA function to rescue the expression of genes with the DxE motif. When ribosomes encounter repeats of acidic residues (adjacent or separated by one residue) during the early stage of the synthesis of the nascent elongating peptide, they stall and in certain cases, they dissociate from the mRNA (as for *aceB* and *mgtL* genes). EttA can probe stalled ribosomes with an empty E site and restore the elongation process, then it dissociates using its ATPase activity. **e**, Structure of EttA-EQ₂ (dark blue) in complex with 70S IC complex (EMD-29398)²³ aligned on the domain V of the 23S rRNA of the structure (6ENJ)⁷⁰ of the polyproline-stalled ribosome in complex with EF-P (green).

METHODS

Bacterial strains

The strains used in this study are listed in **Supplementary Tables 1 to 3**. The WT reference strain used was the sequenced MG1655⁹² strain. The $\Delta ettA$ strain from a previous study⁶ was complemented by insertion of the *ettA* gene with its native promoter at the P21 genomic locus (strain C_{ettA}) or at the *attB* locus (strain C'_{ettA} , this strain was used for the Δicd constructions because the P21 locus was not compatible with this deletion). The insertion comprises the ORF of EttA with 105 base pairs upstream and downstream. Insertions in the genome were conducted using the pOSIP clonetegration recombination method⁹³. Primers used for the amplification and control of the insertion are described in **Supplementary Table 5**. Strains harboring a *yfp* fusion with the *aceA*, *aceB*, *fumA*, *fumB*, *fumC*, *frdA*, *frdB*, *frdD*, *mgo* and *glcB* genes were constructed by P1 transduction using a collection of YFP fusions created by the Mori laboratory⁹⁴ as donor strains and the three receiver strains MG1655 (WT), $\Delta ettA$ and C_{ettA} . Strains harboring a *yfp* fusion with the *yjbJ*, *hchA* and *elaB* genes were constructed by amplifying the *yfp* and chloramphenicol resistance cassettes from the Mori collection⁹⁴ with primers containing in their 5' extremities 60 base pairs homologous to the upstream and downstream regions of the stop codon of the target gene (**Supplementary Table 5**). Then, the PCR products were introduced by electroporation into MG1655 cells harboring a plasmid (pKD46) expressing the λ_{red} recombinase and the Gam proteins⁹⁵ followed by a selection of chloramphenicol-resistant fusion clones. The constructs were finally transduced with P1 phage into the receiver strains (WT, $\Delta ettA$ and C_{ettA}). For the strains individually deleted of *ettA* target genes, deletions from donor strains of the

Keio collection⁹⁶ were transferred by P1 transduction into the receiver strains (WT, Δ *ettA*, *C_{ettA}* and *C[']_{ettA}*). All the constructed strains were verified by PCR using the primers described in **Supplementary Table 5**.

Plasmids construction

All the plasmids constructed in this study are listed in the **Supplementary Table 4** and were cloned in the DH5 α strain. The pMMB plasmids used for target validation in the WT, Δ *ettA*, and *C_{ettA}* strains, were derived from the low-copy plasmid pMMBpLacO-1-67EH-. It allows controlled gene expression from the IPTG inducible PLlacO-1 promoter³³ with a transcription start that permits to retain the native 5'UTR of the inserted gene. All of *EttA* target genes, (except the *mgtL_mgtA_{1-5aa}* insert sequence, which was synthesized by the company TWIST bioscience) were PCR amplified from genomic DNA of the MG1655 strain with primers hybridizing at the transcription initiation site and to the stop codon of the ORF. In the case of multiple transcription start sites we selected the one that generates the shortest 5'UTR. The primers and the synthetic insert have in their extremities an homology (15 to 20 bases) to the PCR products of the pMMB produced for the cloning (**Supplementary Table 6**). The plasmids were assembled using the NEBuilder HiFi DNA Assembly kit (New England BioLabs). The different truncated or point mutants derived from these plasmids were generated by PCR amplification using primers (**Supplementary Table 6**) that hybridize at the truncation or contain the point mutations(s) and with 15 bases of homology to allow plasmid recircularization using the NEBuilder HiFi DNA Assembly kit. The pMMB-*aceB* and pMMB-*aceA* plasmids without the YFP fusion were also generated by the same strategy. Plasmid constructs carrying the nucleotide sequence encoding the NKDEPD motif were generated from the plasmid pMMB-*aceB*-NQ:*yfp* by the same approach. The synonymous coding sequence for pMMB-UTR_{*yjbJ*} MNKDEPD_{syn-codon:*yfp*} changes the original sequence ATGAATAAAGATGAACCAGAT to ATGAATAAAGACGAGGCCAGAC where the three codons encoding acidic residues were replaced by synonymous codons (codons encoding the same residues). All the constructed plasmids were confirmed by sequencing. Most of the constructions with a *yfp* gene express the native YFP venus except for the *mgtL_mgtA* constructions which express an optimized YFP³³ and of the *yfp* mutant presented in **Extended Data Fig. 7a** where the first 6 codons systematically use the synonymous codon with the highest number of adenosine.

Growth media and culture conditions

Overnight cultures of the various MG1655 strains were carried out in Luria-Bertani Miller broth (LB-Difco) at 37 °C with agitation. For strains transformed with pMMB or pBAD plasmids, growth medium was supplemented with ampicillin at 100 μ g.ml⁻¹ (LB_Amp100) or kanamycin at 50 μ g.ml⁻¹ (LB_Kan50) and, when required, 0.4% (w/v) of β -D-glucose was added to repress expression of pBAD plasmids (pBAD-*His₆-ettA*-EQ₂). Bacteria were cultivated in the different media indicated in the figures. A modified MJ9 medium⁹⁷, composed of KH₂PO₄ at 16.5 mM, K₂HPO₄ at 8.5 mM, NH₄SO₄ at 15 mM, MgSO₄ at 2 mM, MOPS at 133 mM, Tricine at 13.3 mM, supplemented by a 100X dilution of a vitamins mix (MEM VITAMINS, Sigma-Aldrich) and trace elements as described in the original MJ9 medium⁹⁷, was used for the cultures. For the MMAA, all the amino acids (Sigma-Aldrich) with the exception of cysteine, tyrosine, tryptophan and methionine (due to their low solubility) were added at 2 mg.ml⁻¹ as carbon source for a final concentration of: glycine at 26.6 mM, alanine at 22.4 mM, valine at 17 mM, leucine at 15.2 mM, isoleucine at 15.2 mM, proline at 17.3 mM, phenylalanine at 12.1 mM, serine at 19 mM, threonine at 16.8 mM, asparagine at 15.1 mM, glutamine 13.7 mM, aspartic acid at 15 mM, glutamic acid at 13.6 mM, arginine at 11.4 mM, histidine at 12.8 mM and lysine at 13.6 mM. Other carbon sources tested were: L-malic acid, sodium fumarate dibasic, succinic acid and pyruvic acid and α -ketoglutaric acid at 0.3 M, glyoxylic acid (MM.Glyoxylate) and oxaloacetic acid at 0.15 M and Glucose at 22 mM (MMGlc) all in the MM medium (carbon sources are purchased from Sigma-Aldrich with the exception of α -ketoglutaric purchased from Bio Basic). For the assay with salt, NaCl was added at the indicated final concentrations in the figures. Expression of the inserted genes or YFP fusions was induced by addition to the medium of 1mM of Isopropyl β -D-1-thiogalactopyranoside (IPTG) for the pMMB constructions or 0.2% (w/v) of L-Arabinose for the pBAD constructions.

Cultures in 96-well Falcon microplates were done in triplicate in a volume of 200 μ l of medium inoculated with 2 μ l of over-night culture (for the MMAA NaCl test, the cultures were washed with a solution of 0.9% (w/v) NaCl prior to inoculation) and a volume of 60 μ l of mineral oil (Sigma Aldrich) was added to each well in order to prevent evaporation of the medium during growth. Growth of the different strains was followed by measuring the optical density at 600 nm (OD_{600}) when incubated at 37 °C under 600 rpm double-orbital shaking with a CLARIOstar plate reader (BMG Labtech). The emission of the YFP fluorescence was recorded at 540-20 nm with an excitation at 497-15 nm. Measurements were taken every 30 min.

Fitness assays

Competitive fitness assays were conducted as described previously⁶ except that different media, described in the **Extended Data Fig. 1a**, were tested (Luria-Bertani (LB) medium from two different providers: Difco Becton Dickinson and USB-affymetrix, MMAA and MMGlc media described above). Briefly, from overnight cultures in LB-Difco medium of the WT and Δ *ettA* strains, an inoculum composed of an equal ratio of the two strains was used to start a co-culture in the media indicated in the **Extended Data Fig. 1a**. Growth was carried out at 37 °C with shaking for a determined period, then the cultures were sub-cultured in fresh medium (+ 24 h) to test the viability of the strains during the experiment. PCR assays were performed on cells at the end of each co-culture, using primers hybridizing at ~500 bp upstream and downstream of the *ettA* gene as previously described⁶.

Motility assay

Stationary-phase bacterial cultures were used for the motility test. Overnight precultures of the three strains (WT, Δ *ettA* and *C*_{*ettA*}) were washed and diluted to an OD_{600} = 0.5 in physiological water to prepare the inoculum. The motility test was then carried out on a plate containing the MMAA culture medium supplemented with 0.3% (w/v) agar. Plates were inoculated by picking them using a toothpick soaked in an inoculum and then incubated at 37°C. Representative images of the swimming motility are shown after 48 h.

Protein extracts and total RNA preparation

Samples for quantification by western and northern blots of protein and mRNA of the *yfp* genomic fusion with *aceA*, *aceB*, *fumC*, *yjbJ* and *hchA* genes were prepared as following. 96-well microplate culture of each strain (WT, Δ *ettA* and *C*_{*ettA*}) with the *yfp* fusion were grown in MMAA or LB medium as described above. For the western blotting, 100 μ l of the culture was pelleted, then resuspended in Laemmli (Bio-Rad), Sample Buffer in a volume to normalize the OD_{600} . For northern blotting, 400 μ l of culture were resuspended in 100 μ l of RNAsnap buffer (95% (v/v) formamide, 18 mM EDTA, 0.025% (v/v) SDS, 1% (v/v) β -mercaptoethanol) using the RNAsnap method as described previously⁹⁸.

Western Blotting

After separation on a 12.5% acrylamide SDS-PAGE gel, proteins were transferred onto a polyvinylidene difluoride (PVDF) membrane for 30 min at 2.5 V and 25 mA using a semi-dry Trans-Blot Turbo system (Bio-Rad). Membranes were blocked by incubating them for two hours at room temperature in a PBS buffer supplemented with 5% (w/v) of skimmed milk powder and then incubated for 2 h at room temperature or overnight at 4 °C in 3 ml of PBS 1X + 0.1% (v/v) Tween-20 in presence of a 1,000x dilution of anti GFP antibody (Rabbit anti-GFP, Invitrogen Thermo Fisher Scientific). After washing, the bound antibody was detected by incubation for 1 h in PBS buffer in the presence of a secondary antibody: for *aceB*, *aceA* and *yjbJ yfp* fusions, a near infrared fluorescent probe (IRDye 680LT anti-rabbit LI-COR Biosciences) diluted 20,000x in PBS was used whereas for *hchA* and *fumC yfp* fusions, an HRP-conjugated antibody (Anti-rabbit IgG, antibody [HRP] from COVALAB) diluted 20,000x in PBS was used. The HRP-conjugated antibody was detected with the Clarity Western ECL Substrate (Bio-Rad) and signal detection was performed on a Licor Odyssey scanner.

Northern Blotting

For each condition, 6 µg of total RNAs were loaded on a 1% (w/v) agarose gel. Electrophoretic migration was carried out for 75 min at 100 V. RNAs were then transferred to an Amersham Hybond-N+ membrane (Cytiva). Transfer of the RNAs was verified by UV. The RNAs were cross-linked on the membrane by exposing the membrane to UV for 30 s at 100 x 1 200 µJ / cm². The radioactive probe was prepared from 40 pmoles of primers described in **Supplementary Table 7** and labeled at the 5' end with 10 units of T4 polynucleotide kinase (New England Biolabs) and [γ -³²P]-ATP (150 µCi). Membranes were incubated with the probe in the hybridization buffer (ULTRAhyb, Invitrogen Thermo Fisher Scientific) overnight at 42 °C. Membranes were washed three times (once in 2x SSC + 0.1% (v/v) SDS, once in 1x SSC + 0.1% (v/v) SDS and finally in 0.1x SSC + 0.1% (v/v) SDS) at 42 °C during 15 min. Radioactive signal was detected on a Typhoon 9 500 FLA scanner (GE Healthcare).

RNA-seq and proteomic experiments

Cultures of the three strains (WT, Δ *ettA* and *C*_{ettA}) in a volume of 125 ml of MMAA 0.4 M NaCl medium were inoculated at 1/20 with overnight cultures prepared in LB-Difco medium. Cells were grown at 37 °C with shaking. After 330 min of culture, 3 ml samples were collected for each strain for the transcriptomic analysis. Cultures were stopped by addition of two volumes of RNAprotect (Qiagen) then centrifuged at 5,000 g for 5 min. Pellets were isolated and immediately stored at - 80 °C. Total RNA were extracted with the Direct-zol RNA MiniPrep kit (ZYMO RESEARCH). Ribosomal RNAs were specifically eliminated using the Ribo-Zero rRNA Removal kit (Illumina). The library and deep sequencing were performed by the GATC company on an Illumina HiSeq sequencer. Sequences were aligned with Bowtie2⁹⁹, indexed with Samtools¹⁰⁰ and counted with FeatureCount¹⁰¹. Normalization and statistical analysis were performed with R software¹⁰² and Deseq script¹⁰³.

For the proteomic experiments, sample of 100 ml were taken from triplicated cultures. Cells were washed in PBS and pelleted by centrifugation at 5,000 xg for 10 min at 4 °C. Pellets were resuspended in 150 µl of the lysis buffer (PBS 1X, 1% protease inhibitor cocktail EDTA-free, Roche-100X in DMSO and lysed by sonication (amplitude 70%, 3 pulses of 15 sec separated by 15 sec intervals). Two proteomics analyses were performed, named “proteomic S₁₅” and “proteomic P₁₅₀” respectively. First, for the proteomic S₁₅, lysates were centrifuged at 15,000 g for 30 min at 4 °C and protein extracts were recovered and divided into 3 aliquots of 50 µl. The concentrations of the protein extracts were determined using a BCA assay (Pierce BCA Protein Assay, Thermo Fisher Scientific) and a verification of the protein extracts was carried out on a 12.5% acrylamide SDS-PAGE gel stained with Coomassie brilliant blue R-250. 25 µg of each protein sample were diluted in a final volume of 25 µl for a final concentration of 8 M Urea / 50 mM Ammonium Bicarbonate. Cysteine reduction and alkylation were achieved by the addition of DL-Dithiothreitol and iodoacetamide respectively. The protein extracts were digested by Lys-C endoproteinase and then by trypsin (Trypsin Gold, Promega). Peptides were vacuum- dried and resuspended in 100 µl of solvent A (0.1% (v/v) formic acid in 3% (v/v) acetonitrile) to get a final concentration of 250 ng.µl⁻¹ before analysis by MS / MS mass spectrometry. For the proteomic P₁₅₀, lysates were centrifuged at 150,000 g for 1 hour at 4 °C. Pellets were resuspended in 200 µl of 1X PBS with 0.3% (v/v) SDS and the concentrations of the protein extracts were determined using a BCA assay. 25 µg of each sample were loaded on a 12.5% acrylamide SDS-PAGE gel and after a short (1 cm) migration, proteins were stained with Coomassie brilliant blue R-250. Lanes containing proteins were excised and subjected to digestion with porcine trypsin. Protein extracts were then processed in the same way as protein extracts from proteomic S₁₅.

Mass spectrometry analyses were performed on a Q-Exactive Plus hybrid quadrupole-orbitrap mass spectrometer (Thermo Fisher, San José, CA, USA) coupled to an Easy 1,000 reverse phase nano-flow LC system (Proxeon) using the Easy nano-electrospray ion source (Thermo Fisher). Briefly, peptide mixtures were analyzed in triplicate. 4 µl of peptide mixtures were loaded onto an Acclaim PepMap precolumn (75 µm x 2 cm, 3 µm, 100 Å; Thermo Scientific) equilibrated in solvent A and separated at a constant flow rate of 250 nl/min on a PepMap RSLC C18 Easy-Spray column (75 µm x 50 cm, 2 µm, 100 Å; Thermo Scientific) with a 90 min gradient (0 to 20% solvent B (0.1% (v/v) formic acid in acetonitrile) in 70 min and 20 to 37% solvent B in 20 min). Data acquisition was performed in positive and data-dependent modes.

Full scan MS spectra (mass range m/z 400-1800) were acquired in profile mode with a resolution of 70,000 (at m/z 200) and MS/MS spectra were acquired in centroid mode at a resolution of 17,500 (at m/z 200).

Data processing for label-free quantification - Raw data were processed with the MaxQuant software package (<http://www.maxquant.org>, version 1.5.6.5)¹⁰⁴. Protein identifications and target decoy searches were performed using the Andromeda search engine and the SwissProt database restricted to the *E. coli* K-12 taxonomy (release: 15/11/2018; 4477 entries) in combination with the Maxquant contaminants database (number of contaminants: 245). The mass tolerance in MS and MS/MS was set to 10 ppm and 20 mDa, respectively. Methionine oxidation and protein N-term acetylation were taken into consideration as variable modifications whereas cysteine carbamidomethylation was considered as fixed modification. Trypsin was selected as cutting enzyme and 2 missed cleavages were allowed. Proteins were validated if at least 2 unique peptides having a protein FDR < 0.01 were identified. The setting "Match between runs" was also taken into consideration to increase the number of identified peptides. For quantification, we used unique and razor peptides with a minimum ratio count ≥ 2 unique peptides. Protein intensities were calculated by Delayed Normalization and Maximal Peptide Ratio Extraction¹⁰⁵ (MaxLFQ). Statistical analysis was done using Perseus software (<https://maxquant.org/perseus>, version 1.6.0.7) on LFQ intensities. Proteins belonging to contaminants and decoy databases were filtered. For each biological replicate, the median intensity of the two injected replicates was determined and proteins having quantitative data for all the biological replicates were considered for statistical analysis using a Benjamini-Hochberg test. Principal component analysis of the S₁₅ proteomic result showed an outlier sample for one of the Δ ettA biological triplicate, therefore, it was excluded and the analysis was carried on biological duplicate for the three strains.

Protein expression and purification

EttA and EttA-EQ₂ proteins were expressed with an N-terminal hexahistidine-tag (His₆) from the pBAD plasmid under the control of an arabinose-inducible promoter in the strain MG1655. Protein production and purification was conducted following the previously published method⁶ with the following changes. Cell lysis was performed by 3 successive passages in a cell disrupter (Constant Systems Ltd) at 2.5 kbar pressure. Initial purification step was realized on a Protino Ni-NTA column (Macherey-Nagel) then on a butyl-Sepharose FF (Cytiva) and finally monodispersed purified protein were separated on a HiPrep 16/60 Sephacryl S-200 column (Cytiva). Purification buffers were the same as in Boël *et al.*⁶. The concentration of the protein was estimated using the BCA kit (Pierce BCA Protein Assay Kit - Thermo Fisher Scientific) according to the supplier's recommendations as well as by comparing the protein on a 12.5% acrylamide Coomassie-stained SDS-PAGE gel with BSA standards. The pure protein was frozen in liquid nitrogen and stored at -80 °C.

Purification of *E. coli* MRE600 ribosomes

Highly purified ribosomes of *E. coli* MRE600 strain, devoid of EttA protein (undetectable by Western blotting), were prepared by multiple centrifugations over sucrose cushions and gradients. Briefly, two liters of LB medium were inoculated with 20 ml of a saturated overnight culture of *E. coli* MRE600, grown at 37°C under agitation to an OD₆₀₀ of 0.5. Cells were immediately harvested by centrifugation for 20 min, at 5,000 g at 4 °C then resuspended and washed in buffer A (20 mM Tris pH 7.4, 10 mM Mg(OAc), 100 mM NH₄(OAc), 0.5 mM EDTA). All subsequent steps were performed at 4°C. Cells were resuspended in buffer A supplemented with 0.1 mg.ml⁻¹ lysozyme, 6 mM β -mercaptoethanol and 0.1% (v/v) protease inhibitor cocktail (Sigma Aldrich) and lysed by 3 passages at 2.5 kBar using a cell disrupter (Constant Systems Ltd). Clarification of the lysate was then performed by two centrifugations of the extract at 22,000 g for 20 min at 4°C. The supernatants were recovered and overlaid on an equal volume of 37.7 % (w/v) sucrose cushion in buffer B (20 mM Tris pH 7.4, 10 mM Mg(OAc), 500 mM NH₄(OAc), 0.5 mM EDTA, 6 mM β -mercaptoethanol) and the samples were then centrifuged for 20 h, at 206,000 g at 4°C in a Type 70 Ti rotor (Beckmann Coulter). Sucrose cushions were decanted and the clear ribosomal pellet was resuspended and incubated in buffer C (20 mM Tris pH 7.4, 7.5 mM Mg(OAc), 60 mM NH₄(OAc), 0.5 mM EDTA, 6 mM β -mercaptoethanol) under gentle agitation for 3 h, at 4°C. Then 12 mg of crude ribosomes were loaded onto 10-40% (w/v) sucrose gradients prepared with buffer C and centrifuged for 16 h at 71,935 g at 4 °C in a

SW28 rotor (Beckman Coulter). Gradients were fractionated on a BioComp Piston Gradient Fractionator (BioComp Instruments) and absorbance was measured at 254 nm. Fractions corresponding to the 70S ribosomes were pooled, washed and concentrated in Amicon 50k (Merckmillipore) using Buffer C. The purified ribosomes were quantified by NanoDrop OneC UV-Vis Spectrophotometer (Thermo Scientific) checked on agarose gel, aliquoted, flash frozen in liquid nitrogen and stored at -80 °C.

In vitro transcription

The DNA templates used to generate mRNAs for *in vitro* translation assays and Toeprinting assays, were PCR amplified with primers (**Supplementary Table 7**) from the pMMB plasmids containing the desired genes to be transcribed. The forward primer contains the T7 polymerase promoter sequence (5'-GCGAATTAATACGACTCACTATAGGG-3'). *In vitro* mRNA synthesis was then carried out at 37 °C for 4 h in T7 RiboMAX Large Scale RNA Production System kit (Promega) according to the manufacturer's recommendations. At the end of the reaction, DNA templates were degraded by adding DNase I for 15 min and the mRNA transcripts were purified using TRIzol Reagent (Thermo Fisher Scientific) and Direct-zol RNA Miniprep kit (Zymo Research). The mRNAs were finally eluted in The RNA Storage Solution (Ambion, Thermo Fisher Scientific) and stored at -80 °C.

In vitro translation assays

The PURExpress ΔRibosome In Vitro Protein Synthesis Kit (New England Biolabs) was used for *in vitro* translation assays. Reactions were performed in a final volume of 10 μl according to the instructions given by the manufacturer. This system consists of two solutions A and B in which all elements of the translational machinery are present except the ribosomes. Ribosomes purified from *E. coli* strain MRE600 were used at a final concentration of 2 mM per reaction. In a 10 μl translation reaction, the mRNA encoding each target gene fused with the *yfp* fluorescent reporter gene, was used at a final concentration of 1 μM. The His₆-EttA protein previously diluted to 40 μM in the purification buffer and heated at 37 °C for 4 h (to increase the monomeric conformation) was added to the translation reactions at 5 μM final. As negative control the purified protein was replaced by the purification buffer. Reactions were transferred to a 384-well plate (Sigma Aldrich), incubated for 150 min in the CLARIOstar plate reader (BMG Labtech) and translation of the mRNA was monitored every 2 min by measuring YFP fluorescence as previously described. All the translation assays were performed in triplicate for each condition.

Toeprinting assays

Assays were performed using the PURExpress ΔRibosome (New England Biolabs) according to manufacturer instructions, to determine stalled-ribosome sequence motifs on the target mRNAs. Purified His₆-EttA or His₆-EttA-EQ₂ proteins were added to *in vitro* translation reactions at final concentrations of 2 μM and 5 μM respectively to evaluate the effect of the ABC-F on the stalled ribosomes. In the reactions in which the effect of antibiotics was tested, the antibiotics (thiostrepton or retapamulin) were added first so as to have a final concentration of 50 μM in the tubes and then dried using a SpeedVac vacuum concentrator (Thermo Fisher Scientific). Purified ribosomes from MRE600 were added to the reactions at a final concentration of 2 μM and mRNA templates at 1 μM. Reactions were then incubated at 37 °C for 15 min and 2 pmoles of CY5-labeled primer (**Supplementary Table 7**) complementary to NV1 sequence¹⁰⁶ (5' GGTTATAATGAATTTTGCTTATT 3') were added and incubated immediately for 5 min at 37 °C. Finally, reverse transcription reactions were performed by adding 0.5 μl (corresponding to 5 U) of AMV Reverse Transcriptase (Promega), 0.1 μl dNTP mix (10 mM), 0.4 μl Pure System Buffer (5 mM K-phosphate pH 7.3, 9 mM Mg(OAc), 95 mM K-glutamate, 5 mM NH₄Cl, 0.5 mM CaCl₂, 1 mM spermidine, 8 mM putrescine, 1 mM DTT) for each reaction and incubated at 37 °C for 20 min. Once Cy5-labeled cDNA was generated, the mRNAs were degraded by addition of 0.5 μl of 10 M NaOH and incubation at 37 °C for 20 min. All the reactions were neutralized by addition of 0.7 μl of 7.5 M HCl followed immediately by addition of 20 μl of toeprint resuspension buffer (300 mM Na-acetate pH 5.5, 5 mM EDTA, and 0.5% SDS (v/v)). Using QIAquick Nucleotide Removal kit (Qiagen), cDNAs were purified according to supplier instructions and then dried and resuspended in 6 μl of toeprint loading dye (95% formamide, 250 μM EDTA, and 0.25% (w/v) bromophenol blue). Sanger sequencing reactions were also performed on

the DNA templates that were used for mRNA synthesis for the toeprint assays. Polymerization reactions were prepared in 20 μ l with ddNTPs (625 μ M ddCTP/ddTTP/ddATP or 50 μ M ddGTP), 0.025 U Taq Pol (New England Biolabs), 1x Thermo Pol Buffer (New England Biolabs), 5 nM DNA matrix, 75 nM CY5-labeled primer 137 and 40 μ M of each dNTP. After amplification by PCR, 20 μ l formamide dye was added to each sequencing reaction and all of the samples were denatured at 80 °C for 3 min before being loaded onto the acrylamide/bis-acrylamide/urea sequencing gel. Cy5-labeled cDNAs were detected by fluorescent mode using a Typhoon FLA 9500 (GE Healthcare Life Sciences) Gel Scanner and LPR Ch.2 filter and 635 nm laser.

Analytical gel-filtration and static light-scattering analyses

Protein samples were injected onto a Yarra 3 μ m SEC-2000 (Phenomenex) running at room temperature in 150 mM NaCl, 5% (v/v) glycerol, 20 mM Tris-HCl, pH 7.2. The column effluent was monitored with multi-angle light scattering detector (miniDAWN treos) and refractive index (Optilab T-rEX) detectors from Wyatt Technologies.

Image analyses and preparation

Western and northern blots signals were quantified using Fiji⁸⁹ software. Figures of the structure of EttA-EQ₂ in complex with 70S IC complex (EMD-29398)²³ and structure (6ENJ)⁷⁰ of the polyproline-stalled ribosome in complex with EF-P were prepared using PyMOL Molecular Graphics System (Schrödinger) and the structures were aligned on the domain V of the 23S rRNA.

Statistics and Reproducibility

All the experiments presented have been reproduced at least twice with the same results. The detail of the different statistical analysis presented herein are the following:

Bacteria growth rate -We extracted the early exponential phase of the growth curves, then the doubling time was calculated by fitting the curves to Malthusian growth equation;

$$Y = Y_0 e^{(kt)}$$

$$\text{doubling time} = \frac{\ln(2)}{t}$$

Where Y is the population, Y_0 the starting population, k the rate and t the time. The lag was determined by measuring the delta between the tangent interception with the time axes of the WT strain and compared strain.

Determination of the fluorescence ratio - Calculation of fluorescence ratios were done by first calculating the ratio of the fluorescence to OD₆₀₀ (Fluo/OD) of each triplicate to obtain the normalized fluorescence (FluoN), then the average for the WT, Δ ettA and C_{ettA} strains was corrected by subtracting the average of the FluoN for the WT pMMB-Ø strain (WT strain carrying an empty pMMB plasmid) (FluoN_{control}) to obtain the corrected normalized fluorescence (FluoNC). Finally, we calculated the ratios of the FluoNC for the Δ ettA and the C_{ettA} strains compared to the WT strain. The propagation of uncertainty was determined by the function:

$$f = A - B$$

Where A is the FluoN of the strain WT, Δ ettA or C_{ettA} and B the FluoN_{control}. The resulting standard deviation of the FluoNC was calculated using the equation:

$$\sigma_f = \sqrt{\sigma_A^2 + \sigma_B^2 - 2\sigma_{AB}}$$

Where σ_A and σ_B are the standard deviations of the variables A and B and σ_{AB} the covariance. Finally, the standard deviation of the ratio (σ_r) is:

$$\sigma_r = \frac{FluoNC_{WT}}{\sigma_f}$$

For the fluorescence reporters for *mgtL* or *mgtA* the normalization was done on the WT strain in the 2 mM Mg²⁺ culture condition.

Protein sequence motif analyses - Presence and position of the proteins containing the motif E/D X{0,1} E/D within the first 50 aa of the N-terminal part of the sequence were determined in the *E. coli* proteome using the Ecocyc database¹⁰⁷ and mapped to the proteomic quantification (S₁₅) data (with the EttA targets presented in this study previously excluded). Then the log₂ ratios of the protein quantification ratios for $\Delta ettA$ vs WT and C_{ettA} vs WT were binned into six bins: absence of the motif (N=488 for $\Delta ettA$ vs WT and N=476 for C_{ettA} vs WT), motif between residue 1 to 10 (N=121 for $\Delta ettA$ vs WT and N=116 for C_{ettA} vs WT), motif between residue 11 to 20 (N=204 for $\Delta ettA$ vs WT and N=200 for C_{ettA} vs WT), motif between residue 21 to 30 (N=184 for $\Delta ettA$ vs WT and N=176 for C_{ettA} vs WT), motif between residue 31 to 40 (N=184 for $\Delta ettA$ vs WT and N=177 for C_{ettA} vs WT) and motif between residue 41 to 50 (N=152 for $\Delta ettA$ vs WT and N=150 for C_{ettA} vs WT). Violin plots were generated using Prism 8 (GraphPad) and *p* values were calculated using a two tailed Mann-Whitney test.

Figure 1

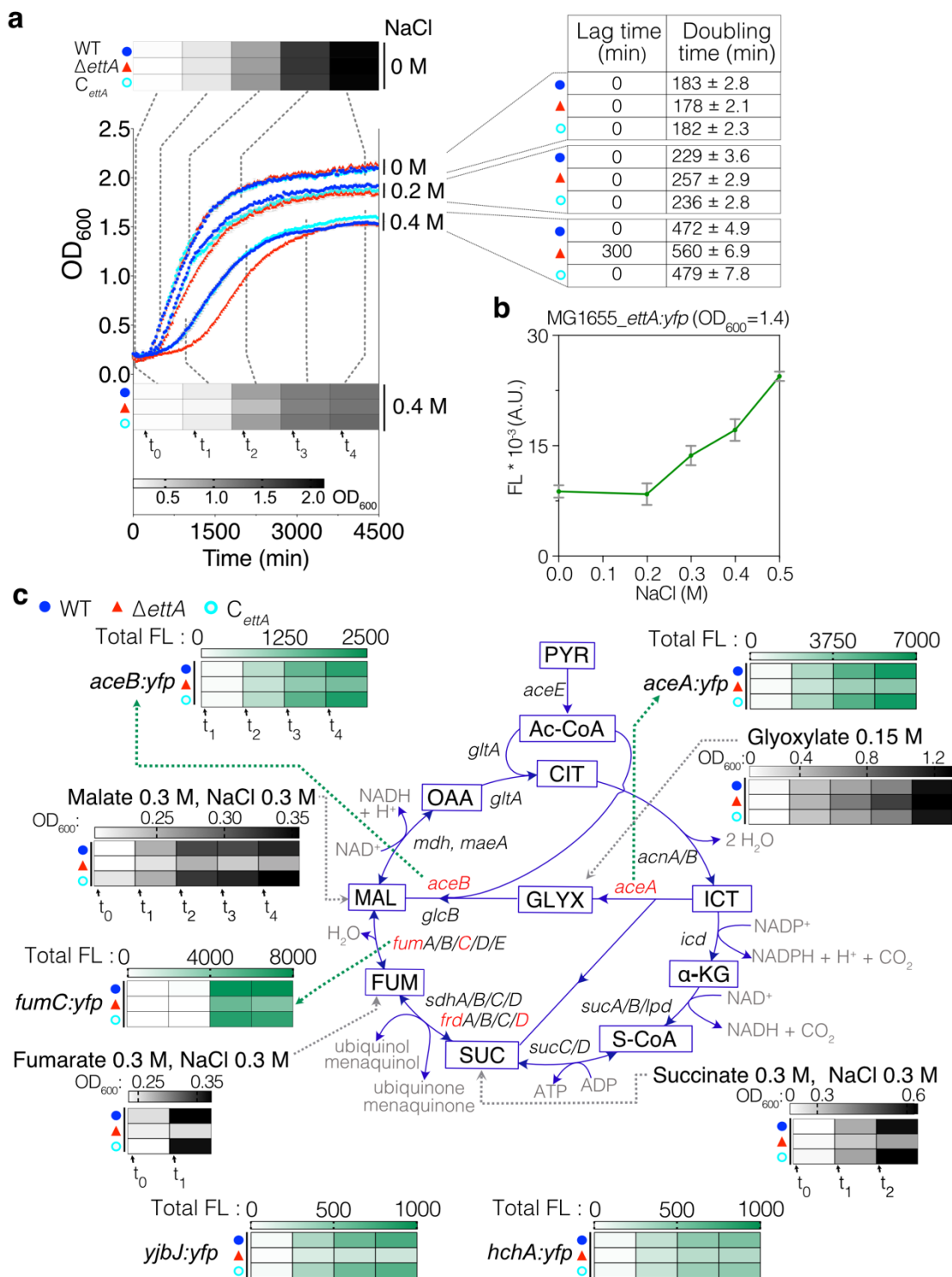


Figure 3

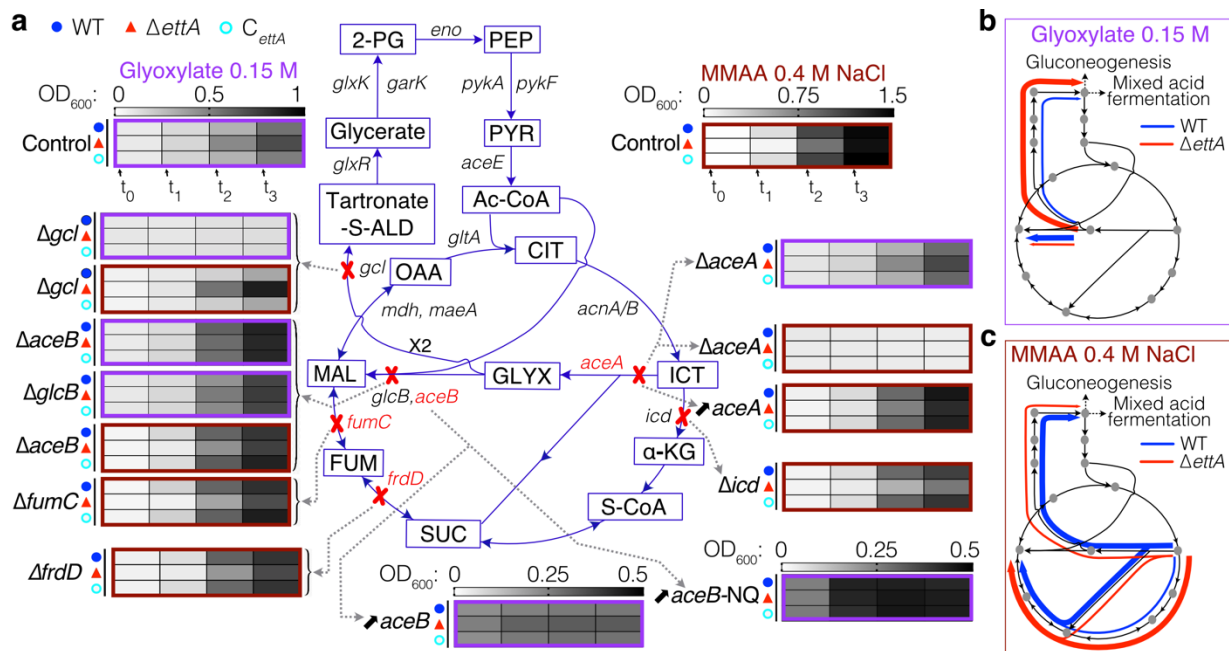


Figure 5

